

**Relic abundance in a secluded dark matter scenario with a massive mediator**Shohei Okawa,<sup>1,\*</sup> Masaharu Tanabashi,<sup>1,2,†</sup> and Masato Yamanaka<sup>3,‡</sup><sup>1</sup>*Department of Physics, Nagoya University, Nagoya 464-8602, Japan*<sup>2</sup>*Kobayashi-Maskawa Institute for the Origin of Particles and the Universe, Nagoya University, Nagoya 464-8602, Japan*<sup>3</sup>*Maskawa Institute, Kyoto Sangyo University, Kyoto 603-8555, Japan*

(Received 13 August 2016; published 25 January 2017)

The relic abundance of the dark matter (DM) particle  $d$  is studied in a secluded DM scenario, in which the  $d$  number decreasing process dominantly occurs not through the pair annihilation of  $d$  into the standard model particles, but via the  $dd \rightarrow mm$  scattering process with a subsequently decaying mediator particle  $m$ . It is pointed out that the cosmologically observed relic abundance of DM can be accomplished even with a massive mediator having a mass  $m_m$  non-negligibly heavy compared with the DM particle mass  $m_d$ . In the degenerated  $d - m$  case ( $m_d = m_m$ ), the DM relic abundance is realized by adjusting the  $dd \rightarrow mm$  scattering amplitude large enough and by choosing an appropriate mediator particle lifetime. The DM evolution in the early universe exhibits characteristic “terrace” behavior, or two-step number density decreasing behavior, having a “fake” freeze-out at the first step. Based on these observations, a novel possibility of the DM model buildings is introduced in which the mediator particle  $m$  is unified with the DM particle  $d$  in an approximate dark symmetry multiplet. A pionic DM model is proposed to illustrate this idea in a renormalizable field theory framework.

DOI: [10.1103/PhysRevD.95.023006](https://doi.org/10.1103/PhysRevD.95.023006)**I. INTRODUCTION**

More than 80% of the matter is made up of dark matter (DM) in the Universe [1–3]. Very little of the DM nature is known, however, besides its cosmological abundance  $\Omega_{\text{dm}} h^2 = 0.1188 \pm 0.0010$  [3].

Theories beyond the standard model (BSM) in particle physics often predict the existence of new massive particles. The lightest neutral stable new particle, if it exists in these BSM scenarios, provides an excellent DM candidate, longevity of which is guaranteed by a new symmetry existing in the BSM scenario. For reviews, see, e.g., Refs. [4,5].

A promising hypothesis we are able to make in these DM models is that the DM particles were produced thermally in the early universe (thermal relic hypothesis) [6] and the cosmological DM abundance can be computed through the Boltzmann equation, once the mass and the couplings of the DM particle are fixed. It has been widely assumed that the DM number density decreasing process was dominated by the pair annihilation of the DM particles into the standard model (SM) particles. If this is true, the DM particle mass and its couplings with the SM particles can be related with each other through the observed value of the cosmological DM abundance. Assuming further the DM pair annihilation cross section is determined by the couplings of the order of the electroweak gauge coupling

strengths, the thermal relic hypothesis predicts the DM particle mass of the weak scale. This striking coincidence is often called the “WIMP Miracle.” The heavier DM particle mass, the stronger DM couplings with the SM sector we need to assume in these widely adopted thermal relic scenarios: we therefore cannot seclude the DM particles from the SM sector. This tendency has encouraged the DM particle searches in the direct detection experiments [7] and in the collider experiments [8]. It is unfortunate, however, up to the present time, we have no fully confidently positive results in these DM particle search experiments [7,9–13].

Recently, new varieties of thermal relic DM scenarios have been proposed. In these scenarios, interactions between the DM particles and the SM particles are weak enough to make the scenarios consistent with the present and near future constraints from the direct DM detections and the collider experiments, still keeping the observed value of the cosmological DM abundance, by introducing novel mechanisms to decrease the DM particle number density in the thermal history of the early universe.

The authors of Refs. [14,15] consider a scenario in which the relic density is controlled by the  $3 \rightarrow 2$  scattering process among the DM particles, instead of the traditional  $2 \rightarrow 2$  process of the DM pair annihilation into the SM particles. The cross section for the  $3 \rightarrow 2$  scattering enough to explain the observed DM abundance may be achieved in the DM model associated with dark strong dynamics, assuming the dark pions to be the DM particle. The anomaly induced Wess-Zumino-Witten (WZW) term [16,17] in the dark chiral Lagrangian naturally explains the required  $3 \rightarrow 2$  scattering in the dark sector. Although

\*okawa@eken.phys.nagoya-u.ac.jp

†tanabash@eken.phys.nagoya-u.ac.jp

‡masato.yamanaka@cc.kyoto-su.ac.jp

the dark sector in this scenario is chemically secluded from the visible sector, it is assumed to interact with the SM sector very weakly, keeping the dark sector temperature equal to the visible sector in the epoch of the DM particle number decreasing processes. It has been pointed out, however, the WZW induced  $3 \rightarrow 2$  scattering annihilation process may not be enough to reduce the DM number density if the higher order effects are incorporated consistently in the chiral perturbation framework.

References [18,19] introduce a phenomenological scenario in which the DM number density decreasing mechanism is implemented by the DM pair annihilation into additional non-SM particles (mediator particles) through the  $2 \rightarrow 2$  process (the secluded DM scenario). The mediator is assumed to decay into the SM particles later and is sufficiently lighter than the DM particle. Note here the mass hierarchy between the two separate mass scales (the DM mass  $m_d$  and the mediator mass  $m_m$ ),  $m_d \gg m_m$ , is introduced on an *ad hoc* basis in this scenario. With a large mass gap  $m_d \gg m_m$ , the DM relic abundance is insensitive to the mediator particle  $m$  lifetime. It is assumed that the dark sector decouples chemically from the visible sector in the early epoch of its thermal history, but it follows the visible sector temperature, keeping the kinematical equilibrium with the SM particles.

The authors of Ref. [20] propose a DM sector almost completely decoupled from the SM sector both kinematically and chemically (cannibal DM). Novel mechanisms similar to SIMP and the secluded DM are responsible for the DM particle number decreasing process in the dark sector. Since the dark sector is decoupled from the SM sector almost completely, the DM particle temperature differs from the SM sector in the thermal history of the Universe. Reference [21] considers a similar scenario having the dark sector kinematically decoupled from the visible sector. The late-time decay of new particles into the SM sector, which were produced copiously in the dark sector thermal history, reheats the visible sector and dilutes the DM density.

In this paper, we solve the Boltzmann equation numerically in a toy secluded DM model having a heavy mediator  $m_d \sim m_m$ . The secluded DM having a large mass gap  $m_d \gg m_m$ , as well as the familiar mechanism of the DM pair annihilation into the SM particles, can also be analyzed in this toy model. We point out the seclusion mechanism works well even with  $m_d \sim m_m$  if the mediator lifetime is short enough, in contrast to the original secluded DM proposal having a large mass gap  $m_d \gg m_m$  and a longer lifetime mediator. The hierarchy assumption  $m_d \gg m_m$  made *ad hoc* in Refs. [18,19] is, therefore, not necessary. We notice that the departure of the mediator number density from its thermoequilibrium value causes non-negligible effects in the evaluation of the DM relic density.

Especially, in the  $m_d = m_m$  case with sufficiently strong  $d - m$  interaction, the evolutions of the DM density

exhibits interesting behavior, i.e., two-step DM density decreasing. At the first step, the dark sector chemically decouples from the SM particles, and the DM density is temporarily frozen to a value much higher than usual thermal relic DM scenario (“fake” freeze-out). This is fake because the DM particle still interacts with the mediator particle strongly, and it keeps the chemical equilibrium with the mediator. The next-step DM density decreasing starts when the mediator decay becomes active. The relic abundance of the DM density is therefore controlled by the mediator lifetime. The true freeze-out takes place only after the DM particle decouples from the mediator. The evolution of the DM density thus exhibits characteristic “terrace” structure in this setup as shown in Fig. 1 later.

The realization of the secluded mechanism with  $m_d \sim m_m$  opens a new fascinating window on the DM model buildings, allowing unified descriptions for the mediator and the DM in the secluded scenarios. We give a concrete example of unified description of mediator and DM, in which both mediator and DM particles are realized as the pseudo-Nambu-Goldstone bosons, in a manner similar to the SIMP scenario. We emphasize that the key process in the secluded DM scenario, i.e., the  $2 \rightarrow 2$  process of the DM pair annihilation into mediator particles, is provided by the low energy theorem amplitude and is well under theoretical control in our concrete model.

This paper is organized as follows: In Sec. II, we give a toy model of the secluded DM model. A brief review on the Boltzmann equation we use in our numerical analysis is also described there. The results on the numerical computations on the evolutions of the DM and mediator number densities are presented in Sec. III. We then propose a pionic DM scenario based on our numerical computation in Sec. IV. Section V is devoted for summary and outlook. We ensure comprehension of the numerical evolutions by analytically describing the relevant quantities in the Appendix.

## II. BOLTZMANN EQUATION IN A TOY MODEL FOR SECLUDED DARK MATTER

It is possible to write down a toy model in which several known DM density decreasing mechanisms, such as the familiar thermal relic DM, the cannibal DM with a decaying mediator, and the secluded DM with a mass gap  $m_d \gg m_m$ , are described in a unified manner. The secluded DM scenario with  $m_d \sim m_m$  we consider in this paper can also be implemented in this toy model as well. We here introduce such a toy model and write down the coupled Boltzmann equations governing the evolutions of the DM and the mediator number densities.

### A. A toy model

We introduce two real scalar fields  $\phi_d$  and  $\phi_m$ , which correspond to the DM and mediator particles  $d$  and  $m$ ,

respectively. They interact with each other and also with the SM weak doublet Higgs field  $\phi$ . The model is described by the Lagrangian,

$$\begin{aligned} \mathcal{L}_{\text{toy}} = & \frac{1}{2}(\partial_\mu\phi_d)^2 - \frac{1}{2}m_d^2\phi_d^2 + \frac{1}{2}(\partial_\mu\phi_m)^2 - \frac{1}{2}m_m^2\phi_m^2 \\ & + g_{ddmm}(\phi_d\phi_d)(\phi_m\phi_m) + g_{m\phi^\dagger\phi}m_m\phi_m\phi^\dagger\phi \\ & + g_{dd\phi^\dagger\phi}\phi_d\phi_d\phi^\dagger\phi \\ & + g_{mm\phi^\dagger\phi}\phi_m\phi_m\phi^\dagger\phi, \end{aligned} \quad (2.1)$$

with  $m_d, m_m$  being masses of the DM particle  $d$  and the mediator particle  $m$ , respectively. The longevity of the DM particle  $d$  is protected by the  $Z_2$  symmetry  $\phi_d \leftrightarrow -\phi_d$ .

We know several parameter regions explain the cosmologically observed DM relic abundance in the present toy model.

- (i) If we take the  $m_m$  much heavier than the DM mass,

$$m_m \gg m_d,$$

we can integrate out the  $m$  particle in the Lagrangian and we only have two parameters  $m_d$  and  $g_{dd\phi^\dagger\phi}$ , which can be chosen to obtain the relic abundance. This model is nothing but the conventional Higgs portal DM [22–24], a typical scenario in the familiar thermal relic DM.

- (ii) If we take

$$g_{dd\phi^\dagger\phi} = g_{mm\phi^\dagger\phi} = 0,$$

and very small  $g_{m\phi^\dagger\phi}$ , the dark sector particles  $d$  and  $m$  decouple from the visible sector almost completely and the thermal equilibrium with the visible sector is lost. For

$$m_d \gg m_m,$$

the mediator  $m$  decays into the visible particles after the decoupling between  $m$  and  $d$ , due to the long lifetime of  $m$ ,  $\propto 1/(m_m g_{m\phi^\dagger\phi}^2)$ . In this case,  $g_{ddmm}$  and  $m_d$  can be chosen to obtain the observed relic density. This scenario can be considered as a Higgs portal realization of the cannibal DM model [20].

- (iii) It is also possible to consider a scenario in which both  $g_{dd\phi^\dagger\phi}$  and  $g_{mm\phi^\dagger\phi}$  are nonzero but satisfy

$$g_{dd\phi^\dagger\phi} \ll 1, \quad g_{mm\phi^\dagger\phi} \ll 1.$$

The DM coupling strengths are arranged so as the dark sector to keep its thermal contact with the visible sector even after its chemical decoupling. Similarly to the cannibal DM case, if we take

$$m_d \gg m_m$$

and nonvanishing  $g_{m\phi^\dagger\phi}$ , the DM density decreasing process takes place in the  $dd \rightarrow mm$  scattering process. The coupling  $g_{ddmm}$  and the DM mass  $m_d$  control the relic abundance. This possibility (the secluded DM with a large mass gap) has been known since Refs. [18,19].

Note that the  $g_{dd\phi^\dagger\phi} \ll g_{mm\phi^\dagger\phi}$  model with  $g_{mm\phi^\dagger\phi} \sim 0.1$  and  $g_{ddmm} \sim 0.1$  can also accommodate the appropriate DM relic density. See Ref. [25] for a study of this possibility in the stable mediator limit. It will be dealt with further in a separate publication.

In the following sections, we consider yet another realization to obtain the appropriate relic abundance by choosing the lifetime of the mediator particle  $m$  in a novel parameter region  $m_m \sim m_d$  and  $g_{dd\phi^\dagger\phi} \ll 1$ ,  $g_{mm\phi^\dagger\phi} \ll 1$ , which guarantee the thermal equilibrium between the dark sector and SM fields in the epoch of its chemical decoupling from the SM particles.

## B. Boltzmann equation with a species going out of equilibrium

Here we describe a procedure to obtain the Boltzmann equation for a particle  $i$  valid even when out-of-chemical-equilibrium particles  $j, X$  and  $Y$  are interacting with the particle  $i$ . We restrict ourselves to the case in which all of these particles keep kinematical equilibriums with the thermal bath and feel the same temperature  $T$ . The validity of this assumption in our DM relic density analysis will be discussed later in Sec. III G.

We illustrate the procedure in a simple setup in which only two processes, (i) decay and inverse decay  $i \leftrightarrow XY$ , (ii) scattering process  $ij \leftrightarrow XY$ , are responsible. Using Eq. (5.11) in Ref. [26], the Boltzmann equation for  $i$  is given by

$$\begin{aligned} \frac{dn_i}{dt} + 3Hn_i = & - \int d\Pi_i d\Pi_X d\Pi_Y (2\pi)^4 \delta^{(4)}(p_i - p_X - p_Y) \\ & \times |\mathcal{M}|_{i \leftrightarrow XY}^2 (f_i - f_X f_Y) \\ & - \int d\Pi_i d\Pi_j d\Pi_X d\Pi_Y \\ & \times (2\pi)^4 \delta^{(4)}(p_i + p_j - p_X - p_Y) \\ & \times |\mathcal{M}|_{ij \leftrightarrow XY}^2 (f_i f_j - f_X f_Y), \end{aligned} \quad (2.2)$$

with

$$d\Pi_a = \frac{g_a d^3\mathbf{p}_a}{(2\pi)^3 2E_a} \quad (2.3)$$

denoting a Lorentz invariant phase space for  $a = i, j, X, Y$ . Here  $g_a$  stands for the internal degree of freedom for particle  $a$ . The Hubble rate  $H$  is given by

$$H = 1.66g_*^{1/2} \frac{T^2}{M_{\text{pl}}}, \quad (2.4)$$

where  $g_*$  represents the total number of relativistic degrees of freedom for particles. We use  $g_* = 106.75$  to simplify the numerical analysis throughout the present paper. The Planck mass is denoted by  $M_{\text{pl}}$ .

In order to perform the phase space integrals in Eq. (2.2), we assume the distribution functions  $f_a$  are approximately given by the Maxwell-Boltzmann distribution form,  $f_a = e^{-(E_a - \mu_a)/T}$ . Here  $\mu_a$  represents the value of the chemical potential for  $a$ . The  $\delta$  functions enforce  $E_i = E_X + E_Y$  and  $E_i + E_j = E_X + E_Y$ . Then the distribution functions are rewritten as  $f_i - f_X f_Y = e^{-E_i/T} (e^{\mu_i/T} - e^{(\mu_X + \mu_Y)/T})$ , and  $f_i f_j - f_X f_Y = e^{-(E_i + E_j)/T} (e^{(\mu_i + \mu_j)/T} - e^{(\mu_X + \mu_Y)/T})$ . Note that the number density  $n_a^{eq}$  for a species  $a$  in chemical equilibrium with the thermal bath is given by

$$n_a^{eq} = \frac{g_a}{(2\pi)^3} \int d^3\mathbf{p}_a e^{-E_a/T}.$$

The actual number density  $n_a$  for a species  $a$  out of chemical equilibrium is related with the chemical potential  $\mu_a$  as  $n_a = e^{\mu_a/T} n_a^{eq}$ .

We introduce thermally averaged decay rates and thermally averaged cross sections as follows:

$$\begin{aligned} \langle \Gamma \rangle_{i \leftrightarrow XY} &= \frac{1}{n_i^{eq}} \int d\Pi_i d\Pi_X d\Pi_Y (2\pi)^4 \delta^{(4)}(p_i - p_X - p_Y) \\ &\times |\mathcal{M}|_{i \leftrightarrow XY}^2 e^{-E_i/T}, \end{aligned} \quad (2.5)$$

$$\begin{aligned} \langle \sigma v \rangle_{ij \leftrightarrow XY} &= \frac{1}{n_i^{eq} n_j^{eq}} \int d\Pi_i d\Pi_j d\Pi_X d\Pi_Y \\ &\times (2\pi)^4 \delta^{(4)}(p_i + p_j - p_X - p_Y) \\ &\times |\mathcal{M}|_{ij \leftrightarrow XY}^2 e^{-(E_i + E_j)/T}, \end{aligned} \quad (2.6)$$

where  $v$  is relative velocity of initial particles. The phase space integrals in the Boltzmann equation (2.2) can now be performed. We obtain

$$\begin{aligned} \frac{dn_i}{dt} + 3Hn_i &= -\{e^{\mu_i/T} - e^{(\mu_X + \mu_Y)/T}\} n_i^{eq} \langle \Gamma \rangle_{i \leftrightarrow XY} \\ &- \{e^{(\mu_i + \mu_j)/T} - e^{(\mu_X + \mu_Y)/T}\} n_i^{eq} n_j^{eq} \\ &\times \langle \sigma v \rangle_{ij \leftrightarrow XY} \\ &= -\left\{ n_i - n_i^{eq} \frac{n_X}{n_X^{eq}} \frac{n_Y}{n_Y^{eq}} \right\} \langle \Gamma \rangle_{i \leftrightarrow XY} \\ &- \left\{ n_i n_j - n_i^{eq} n_j^{eq} \frac{n_X}{n_X^{eq}} \frac{n_Y}{n_Y^{eq}} \right\} \langle \sigma v \rangle_{ij \leftrightarrow XY}, \end{aligned} \quad (2.7)$$

which is expressed in terms of the actual number density  $n_a$  and the number density in chemical equilibrium  $n_a^{eq}$ . In the case where species  $X$  and  $Y$  are in chemical equilibrium with the thermal bath,  $n_{X(Y)}/n_{X(Y)}^{eq} = 1$ , the Boltzmann equation (2.7) reduces to a ‘‘familiar’’ form. Once species  $X$  and/or  $Y$  go out of equilibrium, their number densities deviate from equilibrium values, i.e.,  $n_{X(Y)}/n_{X(Y)}^{eq} \neq 1$ , which makes an important difference from the analysis based on the familiar Boltzmann equation. The nonunity ratio  $n_{X(Y)}/n_{X(Y)}^{eq} \neq 1$  can trigger nonequilibrium of species  $i$  even if the rates of the processes  $i \leftrightarrow XY$  and  $ij \leftrightarrow XY$  are faster than the Hubble rate  $H$ .

The assumption we made on the distribution functions  $f_a$  cannot be justified if the departures from their chemical and thermal equilibria are large. It should be noted, however, the validity of this approximation can be guaranteed in the situation in which all of particles  $i, j, X$  and  $Y$  start to deviate from their chemical equilibria almost simultaneously.

### C. Boltzmann equation for the DM-mediator system

We are now ready to derive the Boltzmann equations which determine the evolutions of the number densities of the DM particle  $d$  and the mediator particle  $m$  in our toy model, Eq. (2.1). The number changing processes of the DM and the mediator are

$$\begin{aligned} m &\leftrightarrow \phi^\dagger \phi, \\ dd(mm) &\leftrightarrow \phi^\dagger \phi, \\ dd &\leftrightarrow mm. \end{aligned} \quad (2.8)$$

The interplay between these processes determines the DM relic density.

The Boltzmann equations are derived by implementing the processes (2.8) in (2.7),

$$\begin{aligned} \frac{dn_d}{dt} + 3Hn_d &= -\langle \sigma v \rangle_{dd \leftrightarrow \phi^\dagger \phi} [n_d^2 - (n_d^{eq})^2] \\ &- \langle \sigma v \rangle_{dd \leftrightarrow mm} \left[ n_d^2 - (n_d^{eq})^2 \frac{n_m^2}{(n_m^{eq})^2} \right], \end{aligned} \quad (2.9)$$

$$\begin{aligned} \frac{dn_m}{dt} + 3Hn_m &= -\langle \Gamma \rangle_{m \leftrightarrow \phi^\dagger \phi} [n_m - n_m^{eq}] \\ &- \langle \sigma v \rangle_{mm \leftrightarrow \phi^\dagger \phi} [n_m^2 - (n_m^{eq})^2] \\ &- \langle \sigma v \rangle_{mm \leftrightarrow dd} \left[ n_m^2 - (n_m^{eq})^2 \frac{n_d^2}{(n_d^{eq})^2} \right]. \end{aligned} \quad (2.10)$$

We assumed that the SM Higgs is in chemical equilibrium, i.e.,  $n_\phi = n_\phi^{eq}$ .

Note that, if the mediator couples with the SM particles sizably via  $g_{m\phi^\dagger\phi}$  or  $g_{mm\phi^\dagger\phi}$ , the mediator keeps its chemical equilibrium with the SM Higgs through the decay and inverse decay process  $m \leftrightarrow \phi\phi^\dagger$ , or through the  $mm \leftrightarrow \phi\phi^\dagger$  process. If the chemical equilibrium of the mediator particle lasts until the final DM freeze-out epoch, the mediator can be regarded as a part of background thermal plasma in the  $dd \leftrightarrow mm$  process. In this case, the DM relic density is determined almost solely by  $g_{ddmm}$  and becomes insensitive to the values of  $g_{m\phi^\dagger\phi}$  and  $g_{mm\phi^\dagger\phi}$ .

The situation becomes a bit elaborate, if  $m$  goes out of chemical equilibrium before  $d$  decouples from the mediator  $m$ . All of couplings  $g_{ddmm}$ ,  $g_{m\phi^\dagger\phi}$  and  $g_{mm\phi^\dagger\phi}$  are equally important in the determination of the DM relic abundance in this case.

In the remaining of this section, we analytically derive the critical value of the  $g_{m\phi^\dagger\phi}$  coupling, which separates these two phases.

We include only the  $m$  (inverse) decay process in the Boltzmann equation (2.10) as the reaction between the mediator and the SM fields. This simplification is reasonable, because the decay dominates over the scattering with the SM Higgs when the temperature drops below  $m$  mass. We introduce a variable  $X_m = n_m R^3$ , where  $R$  denotes the scale factor of the Universe. The Boltzmann equation of  $m$  can be rewritten in terms of  $X_m$ ,

$$\frac{dX_m}{dt} = -\frac{1}{2} \langle \Gamma \rangle_{m \leftrightarrow \phi^\dagger\phi} (X_m - X_m^{eq}), \quad (2.11)$$

where we assumed  $m$  and  $d$  keep their chemical equilibrium. We consider a situation that  $\phi_m$  goes out of equilibrium at a time  $t_0$ .  $X_m$  at a time  $t_0 + \Delta t$  ( $\Delta t$  is an infinitesimal time interval) is obtained by solving the Eq. (2.11) as

$$X_m = X_m^{eq} + C e^{-(\Gamma)\Delta t/2}, \quad (2.12)$$

where  $C$  is a constant. As long as the inequality

$$\langle \Gamma \rangle_{m \leftrightarrow \phi^\dagger\phi} \Delta t \gg 1 \quad (2.13)$$

is satisfied,  $m$  immediately goes back to equilibrium. Hence this inequality stands for the equilibrium condition of  $m$ .

In the derivation of the condition (2.13), we implicitly assume that  $X_m^{eq}$  is constant in an interval  $\Delta t$ . It is necessary for justification for the condition (2.13) to guarantee the inequality  $\Delta X_m^{eq}/X_m^{eq} \ll 1$  in  $\Delta t$ .  $\Delta X_m^{eq}/X_m^{eq}$  in  $\Delta t$  is computed as follows:

$$\begin{aligned} \frac{\Delta X_m^{eq}}{X_m^{eq}} &= \frac{\Delta t}{X_m^{eq}} \left\{ R^3 \frac{\Delta n_m^{eq}}{\Delta t} + n_m^{eq} (3\dot{R}R^2) \right\} \\ &= \Delta t \left\{ \frac{\Delta \log n_m^{eq}}{\Delta t} + 3H \right\}. \end{aligned} \quad (2.14)$$

The first term for  $T_0 < m_m$ , where  $T_0$  represents the temperature which  $m$  goes out of equilibrium, is

$$\frac{\Delta \log n_m^{eq}}{\Delta t} = -H \left( \frac{3}{2} + \frac{m_m}{T} \right). \quad (2.15)$$

Thus the inequality  $\Delta X_m^{eq}/X_m^{eq} \ll 1$  is rewritten in terms of  $m_m$  and  $T$  as

$$\begin{aligned} \frac{\Delta X_m^{eq}}{X_m^{eq}} &= \left( \frac{3}{2} - \frac{m_m}{T} \right) \Delta t H \\ &\simeq -\frac{m_m}{T} \Delta t H. \end{aligned} \quad (2.16)$$

The approximation from the first line to the second line holds for  $m_m \gg T$ .

As a result, by combining the conditions (2.13) and (2.16), we find the condition to maintain the equilibrium of  $m$  and the SM fields as

$$\frac{T}{m_m} \frac{\langle \Gamma \rangle_{m \leftrightarrow \phi^\dagger\phi}}{H} \gg 1. \quad (2.17)$$

We can convert the condition in terms of the model parameters as follows:

$$\begin{aligned} \frac{T}{m_m} \frac{\langle \Gamma \rangle_{m \leftrightarrow \phi^\dagger\phi}}{H} &\simeq \left( \frac{g_{m\phi^\dagger\phi}}{10^{-7}} \right)^2 \left( \frac{106.75}{g_*} \right)^{1/2} \left( \frac{100 \text{ GeV}}{T} \right) \gg 1. \end{aligned} \quad (2.18)$$

Hence  $m$  goes out of the equilibrium of  $m$  and the SM fields for  $g_{m\phi^\dagger\phi} \lesssim 10^{-7}$ . The nonequilibrium of  $m$  indirectly gives rise to the  $d$  decoupling from the SM thermal bath via the  $d - m$  scattering. As a result the  $m$  lifetime controls the  $d$  relic density. We will numerically check these results in next section.

Note that there exist scattering processes with SM fermions  $\psi_i$  or SM gauge bosons, e.g.,  $m\phi \leftrightarrow \psi_i \bar{\psi}_i$ ,  $m\phi \leftrightarrow W^+ W^-$ , and so on, and they can contribute to the  $m$  thermalization. These contributions are however negligible. This is understood as follows. As is noted above, key ingredient in our scenario is that  $m$  goes out of the equilibrium between  $m$  and SM fields, which leads nonfamiliar relic density of DM.  $m$  goes out of the equilibrium for  $g_{m\phi^\dagger\phi} \lesssim 10^{-7}$ . As long as  $g_{dd\phi^\dagger\phi} \gtrsim 10^{-4}$  which is minimum value for the  $m$  thermalization, the reaction  $mm \leftrightarrow \phi\phi$  dominates over the scattering processes with SM fermions or SM gauge bosons. Hence we can omit the scattering processes with SM particles via  $g_{m\phi^\dagger\phi}$  coupling.

### III. NUMERICAL RESULTS

We here present our results on the numerical computations for the DM relic density.

The evolutions of  $d$  and  $m$  particles are illustrated in Secs. III A, III B and Sec. III C with numerical results computed at several reference points. We assume  $m_d = m_m$  in these reference points, since the DM evolution behaves quite differently than the scenario with  $m_d \gg m_m$ . Motivated by the unified model of the DM and the mediator, we consider  $g_{dd\phi^\dagger\phi} = g_{mm\phi^\dagger\phi}$  case throughout in this section. We emphasize that all of the results shown below are not affected, however, even if  $g_{dd\phi^\dagger\phi} = 0$  as long as  $g_{ddmm} \neq 0$ ,  $g_{mm\phi^\dagger\phi} \neq 0$ .

The parameter dependences of the DM relic density are shown in Sec. III D and Sec. III E assuming  $m_d = m_m$ . We find that it is necessary to take into account the nonunity ratio  $n_m/n_m^{eq} \neq 1$  in the Boltzmann equations (2.9) and (2.10). The important role of  $n_m/n_m^{eq} \neq 1$  should be emphasized.

In Sec. III F, we plot the parameter regions consistent with the observed DM relic density in the  $r - g_{ddmm}$  plane. Here the mass ratio  $m_m/m_d$  is denoted by  $r$ . We find numerically that, if the lifetime of the mediator particle  $m$  is longer than the DM decoupling time from the mediator, the mass ratio  $r$  cannot exceed  $\sim 0.95$  in order to account for the observed DM relic abundance. On the other hand, if we introduce a lifetime of  $m$  comparable with or shorter than the DM decoupling time, the situation changes drastically. Our mechanism yields the observed DM relic density in the secluded scenario even for a completely degenerated  $d - m$  system, with which we deduce the upper bound on the mediator lifetime.

The validity of the Boltzmann equation (2.7) in which both  $d$ ,  $m$  and Higgs are assumed to feel the same temperature is studied in Sec. III G.

#### A. Evolution example 1

We here give an example of the number density evolutions for the DM and mediator particles. A typical evolution of  $Y_d = n_d/s$  ( $Y_m = n_m/s$ ) is shown in Fig. 1, with  $Y_d$  ( $Y_m$ ) being the number density normalized by the entropy density  $s$  for  $d$  ( $m$ ). The horizontal axis shows  $z = m_d/T$ . The mediator  $m$  and the DM  $d$  are assumed to degenerate in mass  $m_d = m_m = 1$  TeV. We take  $g_{ddmm} = 4$ ,  $g_{m\phi^\dagger\phi} = 2 \times 10^{-9}$ , and  $g_{dd\phi^\dagger\phi} = g_{mm\phi^\dagger\phi} = 1 \times 10^{-3}$  as a reference point in this plot. The Hubble rate  $H$ , thermal averaged decay rate and inverse decay rate of  $m \leftrightarrow \phi^\dagger\phi$  ( $\langle\Gamma\rangle_D$  and  $\langle\Gamma\rangle_{ID}$ ), and interaction rates of  $dd \rightarrow mm$ ,  $mm \rightarrow dd$ , and  $dd \rightarrow \phi^\dagger\phi$  are shown in Fig. 2 with the same parameter set. As we see in Fig. 2, there exist characteristic time scales which play important roles in the determination of the evolutions. They are

- (i) The time scale  $z_{dd\phi^\dagger\phi}$  at which the both DM and mediator go out of chemical equilibrium from the

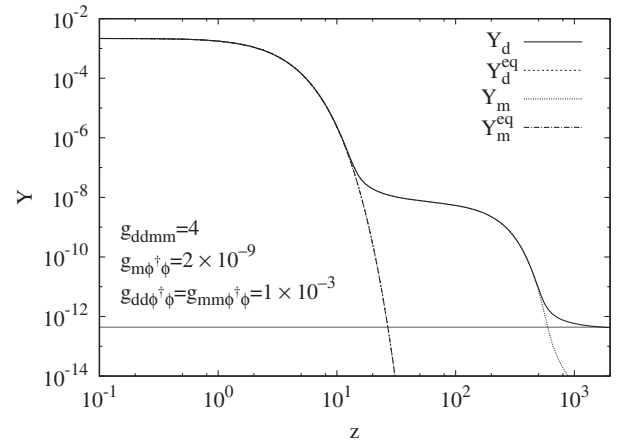


FIG. 1. Evolutions of  $d$  and  $m$ . The observed DM relic density  $Y_d^{\text{obs}} = (4.330 \pm 0.036) \times 10^{-13}$  is shown by the horizontal band.  $m_d = m_m = 1$  TeV,  $g_{ddmm} = 4$ ,  $g_{m\phi^\dagger\phi} = 2 \times 10^{-9}$ , and  $g_{dd\phi^\dagger\phi} = g_{mm\phi^\dagger\phi} = 1 \times 10^{-3}$ .

SM thermal bath. We find it is  $z_{dd\phi^\dagger\phi} \approx 27$  in Fig. 2. This scale can be determined by the condition

$$\langle\sigma v\rangle_{dd\phi^\dagger\phi} n_d = H. \quad (3.1)$$

- (ii) The scale  $z_{m\phi^\dagger\phi} \approx 96$  determined by the mediator lifetime,

$$\langle\Gamma\rangle_D = H. \quad (3.2)$$

The mediator decay starts to affect the evolution of the system after  $z > z_{m\phi^\dagger\phi}$ .

- (iii) The time scale  $z_E$  until when the detailed balance between the  $dd \rightarrow mm$  and  $mm \rightarrow dd$  processes is held. The  $dd \leftrightarrow mm$  detailed balance ends at  $z_E$ . Due to the rapid decreasing of the mediator density through the mediator decay, the mediator density

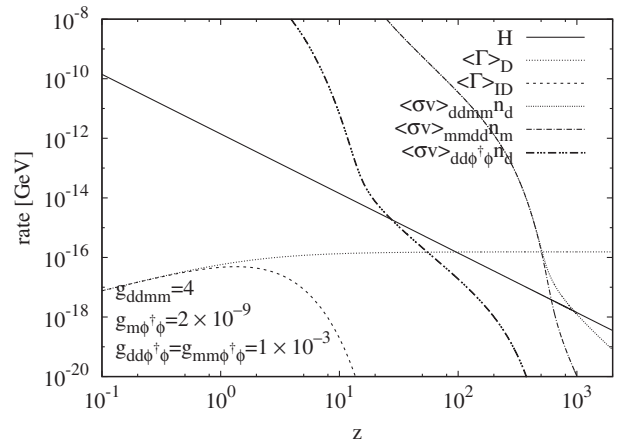


FIG. 2. The Hubble rate  $H$  and interaction rates,  $\langle\Gamma\rangle_D$ ,  $\langle\Gamma\rangle_{ID}$ ,  $\langle\sigma v\rangle_{ddmm} n_d$ ,  $\langle\sigma v\rangle_{m\phi^\dagger\phi} n_m$ , and  $\langle\sigma v\rangle_{dd\phi^\dagger\phi} n_d$ .  $m_d = m_m = 1$  TeV,  $g_{ddmm} = 4$ ,  $g_{m\phi^\dagger\phi} = 2 \times 10^{-9}$ , and  $g_{dd\phi^\dagger\phi} = g_{mm\phi^\dagger\phi} = 1 \times 10^{-3}$ .

$Y_m$  falls below  $Y_d$  after  $z_E$ . The mediator decay rate  $\langle\Gamma\rangle_D$  exceeds the interaction rate of  $dd \leftrightarrow mm$  for  $z > z_E$ . We see  $z_E \approx 510$  with the present set of parameters.

- (iv) The time scale  $z_{ddmm}$  when the  $dd \rightarrow mm$  interaction rate becomes slower than the Hubble rate. The DM density is frozen to its final abundance after  $z_{ddmm}$ , decoupled from the mediator particle  $m$ . We find  $z_{ddmm} \approx 950$  in Fig. 2.

The DM evolution in this setup exhibits distinctive terrace structure as shown in Fig. 1, which can be understood step by step in terms of these characteristic time scales.

In the beginning of the evolution ( $z \ll z_{dd\phi^\dagger\phi} \approx 27$ ), our scenario traces familiar DM evolution in the Higgs portal DM scenario. The DM  $d$  is thermalized through the process  $dd \leftrightarrow \phi^\dagger\phi$  whose rate is much larger than  $H$ . The equilibrium between  $\phi_m$  and the background SM fields is also achieved through the process  $mm \leftrightarrow \phi^\dagger\phi$ .

At the next stage ( $z_{dd\phi^\dagger\phi} \lesssim z \lesssim z_{m\phi^\dagger\phi} \approx 96$ ), the DM density  $Y_d$  is temporarily ‘‘frozen’’ to a value ( $Y_d \sim 10^{-8}$ ) much higher than the corresponding value ( $Y_d \sim 4 \times 10^{-13}$ ) in the well-known Higgs portal DM scenario. We call this phenomenon fake freeze-out of the DM. The larger value of  $Y_d \sim 10^{-8}$  is because the DM interacts with the SM much weaker than the Higgs portal DM in the present model and thus it decouples from the SM at an earlier time. Note that the mediator  $m$  goes out of the equilibrium with the SM simultaneously with the DM fake freeze-out. This situation holds even in the  $g_{dd\phi^\dagger\phi} \ll g_{mm\phi^\dagger\phi}$  case due to the sizable interactions among  $m$  and  $d$ .

The mediator decay becomes active after  $z_{m\phi^\dagger\phi} \approx 96$ . The inverse decay rate  $\langle\Gamma\rangle_{ID}$ , on the other hand, is negligibly small. The  $m$  density in a comoving volume starts to decrease exponentially after  $z \approx z_{m\phi^\dagger\phi}$  through the mediator decay  $m \rightarrow \phi^\dagger\phi$ . The temporarily frozen mediator density  $Y_m$  is then thawed by the mediator decay. We see in Fig. 1, due to the strong interaction  $dd \leftrightarrow mm$ , the DM density  $Y_d$  tracks  $Y_m$  until  $z \approx z_E \approx 510$ . We thus find the DM density  $Y_d$  decreases drastically after its decoupling from the SM thermal bath. It is important to emphasize that the decoupling of  $d$  and  $m$  from the SM thermal bath does not imply the freeze-out of their densities.

Once the  $m$  decay rate exceeds the interaction rate of  $dd \leftrightarrow mm$ , the rapidly decreasing  $m$  density breaks the detailed balance between the interactions  $mm \rightarrow dd$  and  $dd \rightarrow mm$ . Note that the DM density is still decreasing if the interaction rate of  $dd \rightarrow mm$  is larger than the Hubble rate  $H$ . The DM density is fixed to its final abundance only at the last stage ( $z \gtrsim z_{ddmm} \approx 950$ ) when the interaction rate of  $dd \rightarrow mm$  becomes smaller than  $H$ .

## B. Evolution example 2

Another example of typical evolution is shown in Fig. 3, which differs qualitatively from the example we had shown

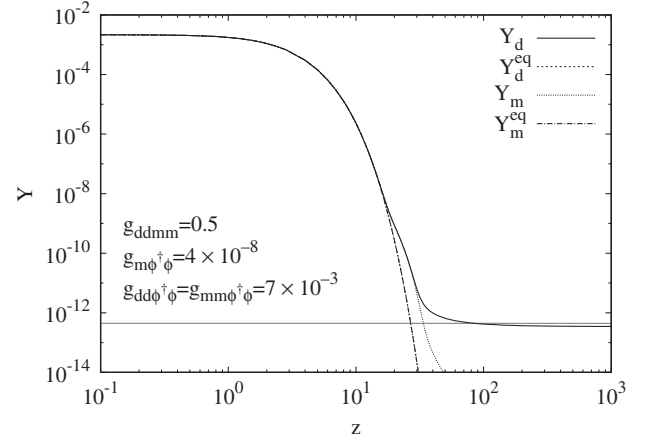


FIG. 3. Evolutions of  $d$  and  $m$ . The observed DM relic density  $Y_d^{\text{obs}} = (4.330 \pm 0.036) \times 10^{-13}$  is shown by the horizontal band.  $m_d = m_m = 1$  TeV,  $g_{ddmm} = 0.5$ ,  $g_{m\phi^\dagger\phi} = 4 \times 10^{-8}$ , and  $g_{dd\phi^\dagger\phi} = g_{mm\phi^\dagger\phi} = 7 \times 10^{-3}$ .

in the previous subsection. In this plot, we take parameters  $m_d = m_m = 1$  TeV,  $g_{ddmm} = 0.5$ ,  $g_{m\phi^\dagger\phi} = 4 \times 10^{-8}$ , and  $g_{dd\phi^\dagger\phi} = g_{mm\phi^\dagger\phi} = 7 \times 10^{-3}$ , which lead to  $z_{dd\phi^\dagger\phi} \approx 23$ ,  $z_{m\phi^\dagger\phi} \approx 6$ ,  $z_E \approx 29$ , and  $z_{ddmm} \approx 56$  as shown in Fig. 4. We therefore find  $z_{dd\phi^\dagger\phi} > z_{m\phi^\dagger\phi}$ , in contrast to the inequality  $z_{dd\phi^\dagger\phi} < z_{m\phi^\dagger\phi}$  we had in the previous subsection. As a result, the distinctive terrace structure we observed in the previous subsection disappears in Fig. 3. Instead, we see a change of slope at the scale  $z_{dd\phi^\dagger\phi}$  in the plot of  $Y_d$ .

## C. Evolution example 3

Here we give an example in which the mediator decay time scale  $z_{m\phi^\dagger\phi}$  coincides approximately with the DM decoupling scale  $z_{dd\phi^\dagger\phi}$ . This situation happens with parameters  $m_d = m_m = 1$  TeV,  $g_{ddmm} = 0.95$ ,  $g_{m\phi^\dagger\phi} = 1 \times 10^{-8}$ ,

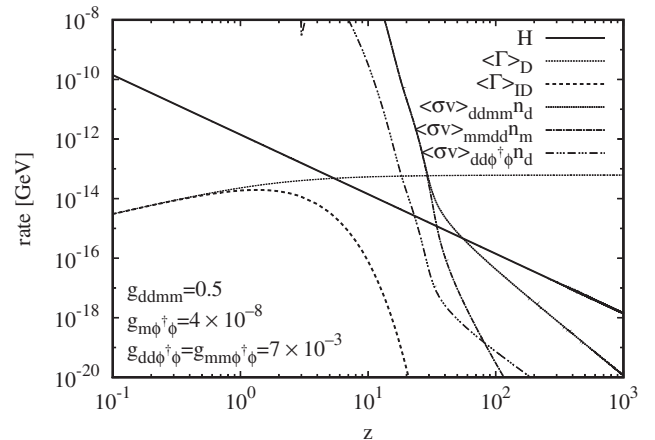


FIG. 4. The Hubble rate  $H$  and interaction rates,  $\langle\Gamma\rangle_D$ ,  $\langle\Gamma\rangle_{ID}$ ,  $\langle\sigma v\rangle_{ddmm}n_d$ ,  $\langle\sigma v\rangle_{m m d d}n_m$ , and  $\langle\sigma v\rangle_{dd\phi^\dagger\phi}n_d$ .  $m_d = m_m = 1$  TeV,  $g_{ddmm} = 0.5$ ,  $g_{m\phi^\dagger\phi} = 4 \times 10^{-8}$ , and  $g_{dd\phi^\dagger\phi} = g_{mm\phi^\dagger\phi} = 7 \times 10^{-3}$ .

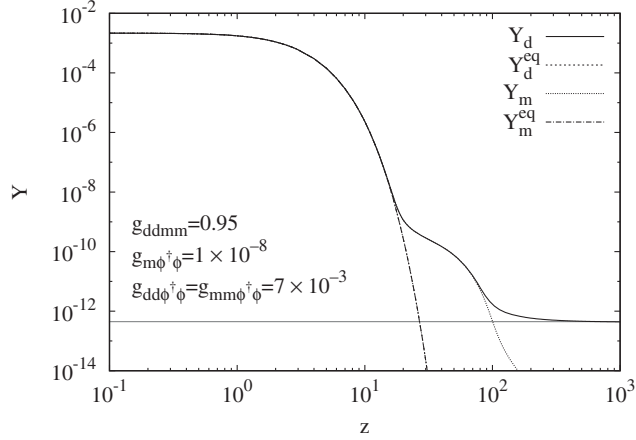


FIG. 5. Evolutions of  $d$  and  $m$ . The observed DM relic density  $Y_d^{\text{obs}} = (4.330 \pm 0.036) \times 10^{-13}$  is shown by the horizontal band.  $m_d = m_m = 1$  TeV,  $g_{ddmm} = 0.95$ ,  $g_{m\phi^\dagger\phi} = 1 \times 10^{-8}$ , and  $g_{dd\phi^\dagger\phi} = g_{mm\phi^\dagger\phi} = 7 \times 10^{-3}$ .

and  $g_{dd\phi^\dagger\phi} = g_{mm\phi^\dagger\phi} = 7 \times 10^{-3}$ . Corresponding time scales are  $z_{dd\phi^\dagger\phi} \approx 31$ ,  $z_{m\phi^\dagger\phi} \approx 20$ ,  $z_E \approx 82$ , and  $z_{ddmm} \approx 152$ . See Fig. 5 and Fig. 6 for the behavior of evolution and interaction rates, respectively. The mediator decay affects the evolution immediately after the DM decoupling from the SM thermal bath. We see no clear terrace structure nor simple slope change in the DM evolution shown in Fig. 5.

#### D. $g_{ddmm}$ dependence

We study the  $g_{ddmm}$  dependence of the  $d$  relic density. Fig. 7 shows the DM relic density as a function of  $g_{ddmm}$ . We take  $m_d = m_m = 1$  TeV. Parameters taken for the analysis are  $(g_{m\phi^\dagger\phi}, g_{dd\phi^\dagger\phi} = g_{mm\phi^\dagger\phi}) = (2 \times 10^{-9}, 1 \times 10^{-3})$ ,  $(2 \times 10^{-9}, 7 \times 10^{-3})$ ,  $(4 \times 10^{-8}, 1 \times 10^{-3})$ ,  $(4 \times 10^{-8}, 7 \times 10^{-3})$ ,  $(1 \times 10^{-8}, 1 \times 10^{-3})$ , and  $(1 \times 10^{-8}, 7 \times 10^{-3})$ , respectively.

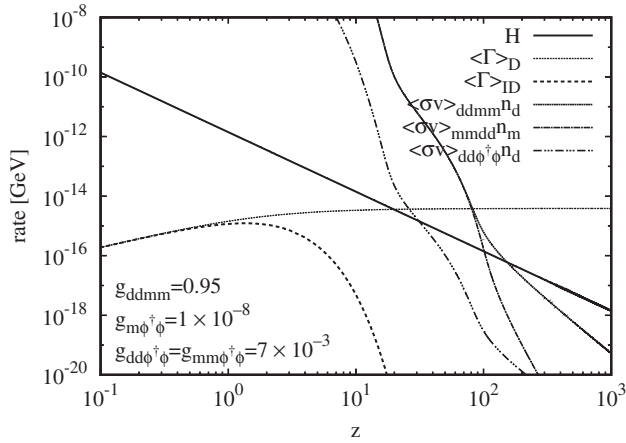


FIG. 6. The Hubble rate  $H$  and interaction rates,  $\langle\Gamma\rangle_D$ ,  $\langle\Gamma\rangle_{ID}$ ,  $\langle\sigma v\rangle_{ddmm}n_d$ ,  $\langle\sigma v\rangle_{m\phi^\dagger\phi}n_d$ ,  $\langle\sigma v\rangle_{m\phi^\dagger\phi}n_m$ , and  $\langle\sigma v\rangle_{dd\phi^\dagger\phi}n_d$ .  $m_d = m_m = 1$  TeV,  $g_{ddmm} = 0.95$ ,  $g_{m\phi^\dagger\phi} = 1 \times 10^{-8}$ , and  $g_{dd\phi^\dagger\phi} = g_{mm\phi^\dagger\phi} = 7 \times 10^{-3}$ .

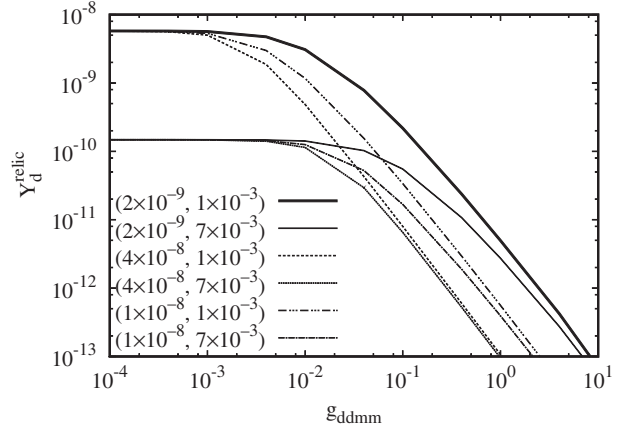


FIG. 7.  $g_{ddmm}$  dependence of  $d$  relic density for each parameter set. Values in the legend represent the parameter set  $(g_{m\phi^\dagger\phi}, g_{dd\phi^\dagger\phi} = g_{mm\phi^\dagger\phi})$ .

Larger  $g_{ddmm}$  provides smaller  $d$  relic density. This is because longer equilibrium between  $d$  and  $m$  can be achieved by larger  $g_{ddmm}$ , which delays the decoupling between  $d$  and  $m$ . As we show in the Appendix, the semianalytic formula (A28) for the DM relic abundance  $Y_d^{\text{relic}}$  is actually inversely proportional to  $g_{ddmm}^2$  and supports this understanding.

On the other hand, smaller  $g_{ddmm}$  gives larger relic density. For each value of  $g_{dd\phi^\dagger\phi}$ , the relic density approaches to its asymptotic value in the  $d - m$  collisionless limit, which corresponds to the DM relic density controlled by the  $g_{dd\phi^\dagger\phi}$  in the Higgs portal scenario. The DM relic density becomes almost insensitive to the value of  $g_{ddmm}$  for  $g_{ddmm} \lesssim g_{dd\phi^\dagger\phi}$ . This is understood as follows. Figure 8 shows the interaction rates of  $dd \rightarrow mm$  and  $dd \rightarrow \phi^\dagger\phi$  for  $g_{ddmm} = 10^{-4}$ ,  $7 \times 10^{-3}$  and 1. Other coupling strengths are taken as  $g_{dd\phi^\dagger\phi} = g_{mm\phi^\dagger\phi} = 7 \times 10^{-3}$  and  $g_{m\phi^\dagger\phi} = 2 \times 10^{-9}$ . We see the DM-mediator decoupling

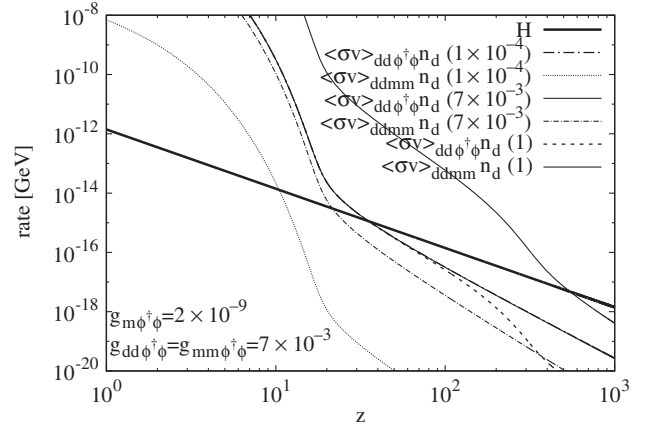


FIG. 8. Comparison of Hubble rate  $H$  and interaction rates of  $dd \rightarrow \phi^\dagger\phi$  and  $dd \rightarrow mm$ . Numbers in the legend represent  $g_{ddmm}$  values.

epoch ( $\langle\sigma v\rangle_{ddmm}n_d = H$ ) is earlier than the DM-Higgs decoupling ( $\langle\sigma v\rangle_{dd\phi^\dagger\phi}n_d = H$ ) for  $g_{ddmm} < g_{dd\phi^\dagger\phi}$ . There is therefore no  $g_{ddmm}$  dependence of the relic density for  $g_{ddmm} \lesssim g_{dd\phi^\dagger\phi}$ .

Hence, our mechanism to reduce the DM relic density works only when the  $g_{ddmm}$  coupling is stronger than the DM-Higgs coupling  $g_{dd\phi^\dagger\phi}$  in the Higgs portal DM scenario.

### E. Mediator lifetime dependence

If the mediator were in chemical equilibrium with the thermal bath,  $Y_m/Y_m^{eq} = 1$  and thus  $n_m/n_m^{eq} = 1$ . The DM Boltzmann equation (2.9) would then be separated from the mediator Boltzmann equation (2.10) completely. The DM relic abundance would therefore be insensitive to the mediator properties such as the mediator lifetime ( $g_{m\phi^\dagger\phi}$  coupling). In the reality, however, the mediator departs from its chemical equilibrium almost simultaneously with the fake freeze-out epoch of the DM. We need to take into account effects of  $Y_m/Y_m^{eq} \neq 1$  in our computations of the DM relic density. Solving the coupled Boltzmann equations (2.9) and (2.10), we obtain the DM relic density as plotted in the solid line in Fig. 9 as a function of  $g_{m\phi^\dagger\phi}$ . On the other hand, if the chemical equilibrium of the mediator particle  $n_m = n_m^{eq}$  were satisfied in (2.9), we would obtain the dotted line result in Fig. 9. We see the coupling  $g_{m\phi^\dagger\phi}$  controls the DM relic density. The effects of the departure of the mediator chemical equilibrium  $Y_m/Y_m^{eq} \neq 1$  are significant.

The relic density decreases with decreasing lifetime (increasing  $g_{m\phi^\dagger\phi}$ ). It approaches to the value of  $Y_m/Y_m^{eq} = 1$  around  $g_{m\phi^\dagger\phi} \approx 10^{-7}$ . The behavior of the relic density is understood as follows. For  $g_{m\phi^\dagger\phi} \gtrsim 10^{-7}$  as derived in Eq. (2.8), the mediator keeps its chemical equilibrium with the SM Higgs. The  $m$  density in (quasi-)equilibrium exponentially drops, and guides the overabundant  $d$  density to the observed one.

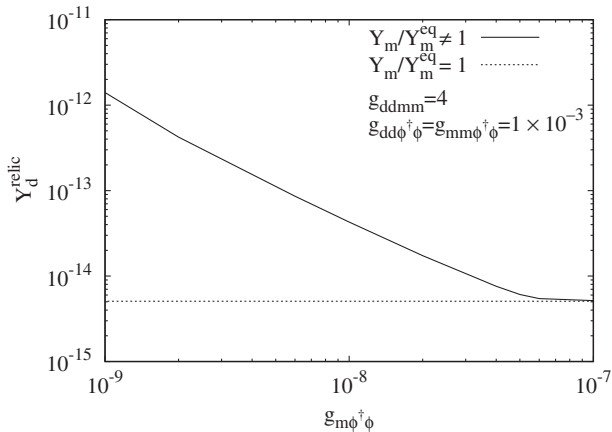


FIG. 9.  $g_{m\phi^\dagger\phi}$  dependence of the DM relic density for  $Y_m/Y_m^{eq} \neq 1$  (solid line) and  $Y_m/Y_m^{eq} = 1$  (dotted line).

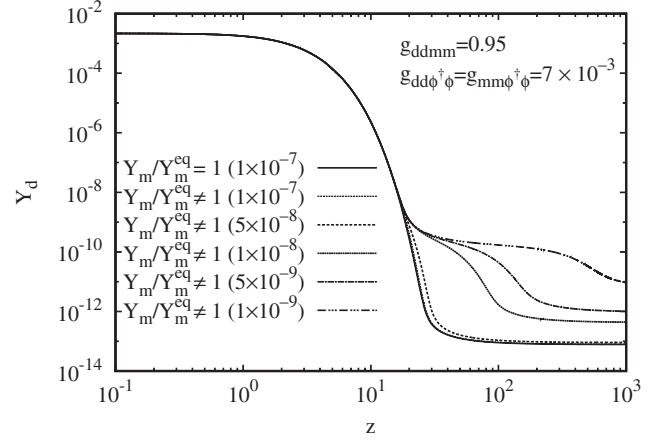


FIG. 10. Comparison of  $d$  evolution for  $Y_m/Y_m^{eq} = 1$  (solid line) and  $Y_m/Y_m^{eq} \neq 1$  (other lines). Numbers in the legend correspond to  $g_{m\phi^\dagger\phi}$  in each calculation.

Figure 10 shows the evolutions of  $Y_d$  for each  $g_{m\phi^\dagger\phi}$ . Too long  $m$  lifetime keeps overdensities of  $m$  for a long period, and leads to a mild damping of  $d$ . Freeze-out of  $Y_d$  occurs at large  $z$  due to a large deviation of  $Y_m/Y_m^{eq}$  from unity, and hence  $Y_d$  remains overabundant. On the other hand, a deviation of  $Y_m/Y_m^{eq}$  from unity becomes smaller for shorter  $m$  lifetime. The Boltzmann equations (2.9) and (2.10) and the relic density approach to those in familiar thermal relic scenarios.

We here note the nonunities  $Y_m/Y_m^{eq} \neq 1$  and  $Y_d/Y_d^{eq} \neq 1$  also affect the evolutions of the  $d$  and  $m$  densities after the epoch  $z_E$ , when the detailed balance of the  $dd \leftrightarrow mm$  process is broken.

### F. Parameter regions consistent with the observed DM relic abundance

We show parameters that can account for the central value of the observed DM relic density  $Y_d^{\text{obs}} = 4.330 \times 10^{-13}$  in Fig. 11. We take  $m_d = 1$  TeV and  $g_{dd\phi^\dagger\phi} = 1 \times 10^{-3}$ . The solid, dashed and dotted lines correspond to the case of negligibly small  $g_{m\phi^\dagger\phi}$  (very late-time decaying mediator),  $g_{m\phi^\dagger\phi} = 2 \times 10^{-9}$  and  $1 \times 10^{-7}$ , respectively. We see in this plot that for  $r \equiv m_m/m_d \lesssim 1/2$  the coupling  $g_{ddmm}$  required for the observed relic density gets close to an asymptotic value  $g_{ddmm} \approx 0.16$ , almost independently of  $g_{m\phi^\dagger\phi}$ . This illustrates the fact that in secluded scenarios with a light mediator ( $r \ll 1$ ), the DM relic density is controlled only by  $g_{ddmm}$  and the DM mass  $m_d$ , and becomes insensitive to  $g_{m\phi^\dagger\phi}$  and  $g_{dd\phi^\dagger\phi}$ .

On the other hand, as  $r$  gets larger, the required coupling  $g_{ddmm}$  also becomes larger. For the case of the negligibly small  $g_{m\phi^\dagger\phi}$  (the very late-time decaying mediator), especially, the coupling  $g_{ddmm}$  goes over the unitarity bound around  $r \gtrsim 0.95$ . We thus find the upper bound on  $r$  so as to explain the observed DM relic density. Thus, with the

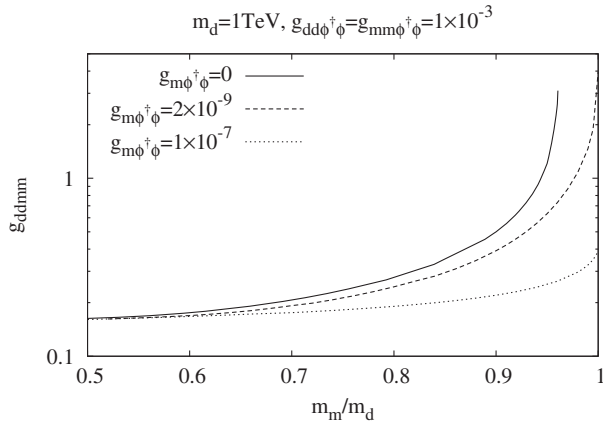


FIG. 11. Parameters reproducing the central value of the observed DM relic density  $Y_d^{\text{obs}} = 4.330 \times 10^{-13}$ . We take  $m_d = 1$  TeV and  $g_{dd\phi^*\phi} = g_{mm\phi^*\phi} = 1 \times 10^{-3}$ . The solid, dashed and dotted lines correspond to the cases with negligibly small  $g_{m\phi^*\phi}$ ,  $g_{m\phi^*\phi} = 2 \times 10^{-9}$ , and  $g_{m\phi^*\phi} = 1 \times 10^{-7}$ , respectively.

extremely long-lived mediator which survives even after the DM decoupling from the mediator, the completely degenerated mediator setup ( $r = 1$ ) is not feasible to account for the observed DM relic density. This property is consistent with the numerical results for the DM relic abundance done in the context of a right-handed sneutrino-neutrino DM-mediator model [27].

The situation changes drastically if we consider a shorter lifetime mediator. The secluded DM scenario with  $r = 1$  becomes viable if the mediator lifetime is comparable with or shorter than the DM decoupling time from the mediator. Actually, when  $g_{m\phi^*\phi} = 2 \times 10^{-9}$ , the coupling  $g_{ddmm} \approx 4$  is required at  $r = 1$  and is marginally consistent with the unitarity. For the mediator with shorter lifetime (larger  $g_{m\phi^*\phi}$ ), it is easier to find the parameter regions consistent with the observed relic density and also with the unitarity. We numerically obtain the lower limit on  $g_{m\phi^*\phi}$ ,  $g_{m\phi^*\phi} \gtrsim 2 \times 10^{-9}$  for  $m_d = 1$  TeV and  $g_{dd\phi^*\phi} = 1 \times 10^{-3}$ .

The required  $g_{ddmm}$  coupling for  $r = 1$  decreases with increasing  $g_{m\phi^*\phi}$ . It approaches to an asymptotic value  $g_{ddmm} \approx 0.4$  around  $g_{m\phi^*\phi} \approx 10^{-7}$ . This is because for  $g_{m\phi^*\phi} \gtrsim 10^{-7}$ , as is described in Sec. II C, the mediator is thermalized through the decay and inverse decay process,  $m \leftrightarrow \phi\phi^\dagger$ , and remains in chemical equilibrium with the SM sector until the final freeze-out of the DM number density. In this case, the DM relic density is insensitive to  $g_{m\phi^*\phi}$  and  $g_{dd\phi^*\phi}$ , and is determined almost through the DM mass  $m_d$ , the DM-mediator mass ratio  $r$  and the  $d - m$  coupling  $g_{ddmm}$ .

### G. Temperature of $d - m$ system

Throughout this work, we assume that the temperatures of  $d - m$  system holds on the background temperature even after they decouple from the SM particles.

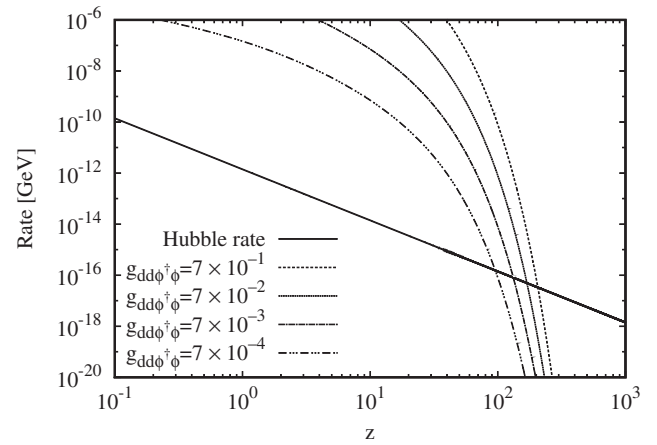


FIG. 12. Hubble rate  $H$  and  $d\phi \rightarrow d\phi$  scattering rate  $\langle \sigma v \rangle_{d\phi \rightarrow d\phi} n_\phi$  for each  $g_{dd\phi^*\phi}$ . We take  $m_d = 1$  TeV.

Kinetic equilibrium of  $d$  and the SM fields ensures that they evolve in a common background with a temperature, even if the chemical equilibrium of them is not achieved. Figure 12 shows the comparison of the Hubble expansion rate  $H$  and the interaction rate of  $d\phi \leftrightarrow d\phi$ . We take  $m_d = 1$  TeV,  $g_{ddmm} = 1$ , and  $g_{m\phi^*\phi} = 1 \times 10^{-8}$ . The interaction rate dominates  $H$  in the region of  $z \lesssim$  a few  $\times 10^2$ . For  $z \gtrsim$  a few  $\times 10^2$ , on the other hand, the dark sector evolves in the temperature  $T_{\text{dark}}$  which may be different from the SM temperature  $T_{\text{SM}}$ .

In the example 1 shown in Sec. III A,  $T_{\text{dark}} = T_{\text{SM}}$  does not hold after the mediator lifetime scale  $z_{m\phi^*\phi}$ . The two-step DM density decreasing profile (terrace behavior) is maintained even if we take into account the effects of  $T_{\text{dark}} \neq T_{\text{SM}}$ , though we neglected the effects in our numerical computations in this paper. The issue will be discussed further in our future publication.

It is also possible to modify our toy model to keep  $T_{\text{dark}} = T_{\text{SM}}$  for a longer period, assuming, e.g., the neutrino portal couplings for the dark sector instead of the Higgs portal coupling.

## IV. A REALIZATION IN PIONIC DARK MATTER SCENARIO

As we have shown in the previous section, the  $dd \leftrightarrow mm$  scattering amplitude needs to be strong enough to achieve the observed DM relic density  $\Omega_{\text{dm}} h^2 = 0.1188 \pm 0.0010$  in our degenerated mediator setup. If we assume the DM and mediator particles are elementary, it is extremely difficult to obtain such a strong interaction without conflicting with the Landau pole problem, however. We here show both of the degeneracy between the DM particle ( $d$ ) and the mediator particle ( $m$ ),  $m_d \approx m_m$ , and the marginally strong interaction in  $dd \leftrightarrow mm$  scattering can be accommodated in models of dark strong dynamics having the dark pions [28–30] as composite particles. Note the dark pions exist ubiquitously in models of electroweak

symmetry breaking, including technicolor [31], composite Higgs [32,33] and also in classically scale invariant extensions of the SM [34–37]. Note also the SIMP mechanism [14,15,38] is embedded in the dark pion scenario, although the DM relic density decreasing mechanism presented in this paper does not rely on it.

### A. Dark QCD and dark pions

We consider a model in which both DM particle  $d$  and mediator  $m$  are unified in a dark pion multiplet. The dark pions are hypothetical pseudo-Nambu-Goldstone bosons associated with dynamical breaking of a newly introduced dark chiral symmetry. They often are the lightest BSM particle existing in models with a dark strong dynamics (dark QCD), and are regarded as the DM candidate particles. In this section, we show the  $d - m$  unification and the marginally strong  $dd \leftrightarrow mm$  amplitude can be achieved in a setup with the dark pions.

We introduce a new strong Yang-Mills gauge dynamics, termed “dark QCD” as

$$\mathcal{L}_{\text{DQCD}} = -\frac{1}{4g_{D_s}^2} G_{\mu\nu}^a G^{a\mu\nu} + \bar{\psi} i \not{D} \psi, \quad (4.1)$$

in analog to the usual quantum chromodynamics (QCD). Here the dark quark fermion field  $\psi$  forms a dark isospin doublet

$$\psi_L = \begin{pmatrix} U_L \\ D_L \end{pmatrix}, \quad \psi_R = \begin{pmatrix} U_R \\ D_R \end{pmatrix}, \quad (4.2)$$

and belongs to the fundamental representation of the dark QCD gauge group. The fermion fields with left- and right-handed chiralities are specified by using subscripts  $L$  and  $R$ , respectively. The Lagrangian (4.1) enjoys global  $SU(2)_L \times SU(2)_R$  dark chiral symmetry,

$$\begin{pmatrix} U_L \\ D_L \end{pmatrix} \rightarrow \begin{pmatrix} U'_L \\ D'_L \end{pmatrix} = \exp\left(i \sum_a \frac{\tau^a}{2} \theta_L^a\right) \begin{pmatrix} U_L \\ D_L \end{pmatrix}, \quad (4.3)$$

$$\begin{pmatrix} U_R \\ D_R \end{pmatrix} \rightarrow \begin{pmatrix} U'_R \\ D'_R \end{pmatrix} = \exp\left(i \sum_a \frac{\tau^a}{2} \theta_R^a\right) \begin{pmatrix} U_R \\ D_R \end{pmatrix}, \quad (4.4)$$

with  $\tau^a$  being the Pauli  $SU(2)$  matrix. In the Lagrangian (4.1), the dark gluon field  $G_\mu^a$  couples with the dark quark  $\psi$  through the covariant derivative,

$$D_\mu \psi = \partial_\mu \psi + i G_\mu^a T^a \psi, \quad (4.5)$$

with  $T^a$  being the fundamental representation matrix of the dark QCD gauge symmetry. The dark gluon field strength  $G_{\mu\nu}^a$  is defined as usual

$$G_{\mu\nu}^a T^a = \partial_\mu G_\nu^a T^a - \partial_\nu G_\mu^a T^a + i G_\mu^a G_\nu^b [T^a, T^b]. \quad (4.6)$$

Note here that both the dark fermion and the dark gluon are blind to the SM gauge group. These fields therefore contribute to the dark component in the Universe.

The negative beta function in the Yang-Mills theory renormalization group equations makes the dark QCD gauge coupling strength  $g_{D_s}$  nonperturbatively strong and induces very strong attractive force between  $\psi$  and  $\bar{\psi}$ , which triggers a  $\bar{\psi}\psi$  condensate

$$\langle \bar{\psi}\psi \rangle \neq 0 \quad (4.7)$$

and dynamical breaking of the dark chiral symmetry,

$$SU(2)_L \times SU(2)_R \rightarrow SU(2)_V, \quad (4.8)$$

in a manner similar to the usual QCD.

It is now apparent how dark pions  $\pi_D^a$  ( $a = 1, 2, 3$ ) appear in this setup. They are the Nambu-Goldstone bosons associated with the dynamical symmetry breaking (4.8). Due to the exact chiral symmetry, however, the dark pions remain exactly massless in this model. We therefore introduce explicit symmetry breaking terms,

$$\mathcal{L}_{\text{explicit}} = -\bar{\psi}_L m_\psi \left( 1 - \frac{1}{\Lambda_s^2} \phi^\dagger \phi - \frac{1}{\Lambda_p^2} i \tau^3 \phi^\dagger \phi \right) \psi_R + \text{H.c.}, \quad (4.9)$$

with  $\phi$  denoting the  $SU(2)_W$  doublet SM Higgs field. The explicit breaking terms, Eq. (4.9), make the dark pions massive. The dark pions interact with the SM Higgs field  $\phi$  also through the explicit breaking terms, Eq. (4.9). Possible origin of these explicit symmetry violating terms, Eq. (4.9), will be dealt in the next subsection in a renormalizable field theory framework. In this subsection, we concentrate on the impacts of these terms in the dark pion phenomenologies.

The dark pion low energy effective theory can be described by using the chiral Lagrangian,

$$\mathcal{L}_\chi = \frac{f^2}{4} \text{tr}[\partial_\mu U^\dagger \partial^\mu U] + \frac{f^2}{4} \text{tr}[\chi^\dagger U + U^\dagger \chi], \quad (4.10)$$

with  $f$  being the dark pion decay constant. Here the nonlinear chiral field  $U$  is expressed using the dark pion field  $\pi_D$ ,

$$U = \exp\left(\frac{i}{f} \sum_a \tau^a \pi_D^a\right). \quad (4.11)$$

The effects of the explicit violation of the dark chiral symmetry, Eq. (4.9), can be analyzed by using

$$\chi = 2Bm_\psi \left( 1 - \frac{1}{\Lambda_s^2} \phi^\dagger \phi + \frac{1}{\Lambda_p^2} i \tau^3 \phi^\dagger \phi \right), \quad (4.12)$$

with  $B$  being a low energy constant related with the dark quark pair condensate.

Expanding the chiral Lagrangian (4.10) in terms of the dark pion field  $\pi_D$ , we obtain

$$\begin{aligned} \mathcal{L}_\chi &= \frac{1}{2} \sum_a (\partial_\mu \pi_D^a) (\partial^\mu \pi_D^a) - \frac{1}{2} m_{\pi_D}^2 \sum_a \pi_D^a \pi_D^a \\ &+ g_{\pi_D \pi_D \phi^\dagger \phi} \sum_a \pi_D^a \pi_D^a \phi^\dagger \phi \\ &+ g_{\pi_D^3 \phi^\dagger \phi} m_{\pi_D} \pi_D^3 \phi^\dagger \phi + \dots \end{aligned} \quad (4.13)$$

It should be noted here that all of the dark pions  $\pi_D^1, \pi_D^2, \pi_D^3$  share the identical mass  $m_{\pi_D}$ , which can be evaluated by using the low energy constant  $B$  and the dark quark mass  $m_\psi$ ,

$$m_{\pi_D}^2 = 2Bm_\psi. \quad (4.14)$$

We also find the dark pions couple with the SM Higgs boson through Eq. (4.9) as

$$g_{\pi_D \pi_D \phi^\dagger \phi} = \frac{1}{2} \frac{m_{\pi_D}^2}{\Lambda_s^2}, \quad (4.15)$$

which plays an important role to thermalize the dark pions in the early universe.

Note that the Lagrangians, Eq. (4.1) and Eq. (4.9), are invariant under the fermion transformation,

$$U_L \rightarrow -U_L, \quad U_R \rightarrow -U_R, \quad (4.16)$$

which also survives as an exact symmetry even after the dynamical chiral symmetry breaking. It is easy to see that  $\pi_D^1$  and  $\pi_D^2$  are odd under the transformation (4.16)

$$\pi_D^1 \rightarrow -\pi_D^1, \quad \pi_D^2 \rightarrow -\pi_D^2. \quad (4.17)$$

They are therefore stable and can be considered as the DM candidate particles. On the other hand, the third component of the dark pion  $\pi_D^3$  is even under the symmetry (4.16). It then decays into the SM Higgs bosons through the coupling

$$g_{\pi_D^3 \phi^\dagger \phi} = \frac{f m_{\pi_D}}{\Lambda_p^2}. \quad (4.18)$$

We identify the third component dark pion  $\pi_D^3$  as the mediator in the secluded DM scenario. In this manner, the DM and the mediator particles are unified in the same dark isospin multiplet. The dark pion scattering amplitude can be evaluated by using the low energy theorem,

$$\begin{aligned} \mathcal{M}(\pi_D^1 \pi_D^1 \leftrightarrow \pi_D^3 \pi_D^3) &= \mathcal{M}(\pi_D^2 \pi_D^2 \leftrightarrow \pi_D^3 \pi_D^3) \\ &= \frac{s - m_{\pi_D}^2}{f^2}. \end{aligned} \quad (4.19)$$

The amplitude (4.19) is strong enough to make the secluded DM scenario based on this setup. If we deduce the  $ddmm$  interaction coupling  $g_{ddmm}$  of Eq. (2.1) from the  $\pi_D^1 \pi_D^1 \leftrightarrow \pi_D^3 \pi_D^3$  amplitude at the threshold, we obtain

$$4g_{ddmm} = \frac{3m_{\pi_D}^2}{f^2}. \quad (4.20)$$

The marginally strong amplitude  $g_{ddmm} \sim 1$  can thus be easily achieved for the massive dark pions with  $m_{\pi_D} \sim f$ . The other phenomenological couplings  $g_{m\phi^\dagger\phi}$ ,  $g_{dd\phi^\dagger\phi}$  and  $g_{mm\phi^\dagger\phi}$  are

$$g_{m\phi^\dagger\phi} = g_{\pi_D^3 \phi^\dagger \phi}, \quad g_{dd\phi^\dagger\phi} = g_{mm\phi^\dagger\phi} = g_{\pi_D \pi_D \phi^\dagger \phi}. \quad (4.21)$$

Note that the dark baryons also potentially contribute to the DM relic abundance in this model. The dark baryon relic abundance turns out, however, to be negligibly small in its minimal setup of the dark QCD at the TeV scale, as demonstrated in the technibaryon context in Ref. [39]. In models of asymmetric dark baryon DM, our mechanism to decrease the dark pion number density can be applied to make the dark pions harmless in the cosmology [40,41].

## B. A UV completion

The purpose of this subsection is to give a possible renormalizable UV completion behind the explicit breaking terms, Eq. (4.9). For such a purpose, we introduce real scalar fields  $S$  and  $P$ , which interact with the dark fermions through the Yukawa Lagrangian

$$\mathcal{L}_{\text{Yukawa}} = -\bar{\psi}_L y (S + i\tau^3 P) \psi_R - \bar{\psi}_R y (S - i\tau^3 P) \psi_L, \quad (4.22)$$

with  $y$  being the Yukawa coupling strength. Note that the Yukawa Lagrangian violates explicitly the  $SU(2)_L \times SU(2)_R$  symmetry down to  $U(1)_L \times U(1)_R$ .

We introduce kinetic and potential terms for these scalar field in a renormalizable manner,

$$\mathcal{L}_{LM} = \frac{1}{2} (\partial_\mu S)^2 + \frac{1}{2} (\partial_\mu P)^2 - V(S, P), \quad (4.23)$$

with

$$\begin{aligned} V &= \frac{\lambda}{4} (S^2 + P^2 - F^2)^2 \\ &+ \frac{1}{4} \epsilon_\Delta F^2 (S^2 - P^2) - \epsilon_S F^3 S - \epsilon_P F^3 P, \end{aligned} \quad (4.24)$$

with  $F$  being a constant with a mass dimension. We also introduce the interaction among  $S$ ,  $P$  and the SM Higgs field  $\phi$  as

$$\mathcal{L}_{\phi^\dagger\phi} = -\frac{\lambda_M}{2}(S^2 + P^2)\left(\phi^\dagger\phi - \frac{v^2}{2}\right). \quad (4.25)$$

Note that the dimension 4 operators in the potential (4.24) and the interaction with the SM Higgs (4.25) respect the  $U(1)$  symmetry among  $S$  and  $P$ , while the operators with lower dimensions violate the  $U(1)$  symmetry. The dimension 2 operators respect the symmetries  $S \rightarrow -S, P \rightarrow -P$ , while the dimension 1 operators do not. The potential is arranged to give nonvanishing vacuum expectation values (VEVs) for  $S$  (and  $P$ ) around the  $F$  scale. It is convenient if we parametrize VEVs as

$$\langle S \rangle = \bar{\varphi} \cos \bar{\theta}, \quad \langle P \rangle = \bar{\varphi} \sin \bar{\theta}. \quad (4.26)$$

We also rewrite the explicit symmetry violating parameters  $\epsilon_S$  and  $\epsilon_P$  using new parameters  $|\epsilon|$  and  $\theta_\epsilon$ ,

$$\epsilon_S = |\epsilon| \cos \theta_\epsilon, \quad \epsilon_P = |\epsilon| \sin \theta_\epsilon. \quad (4.27)$$

Note here that, if we take  $\theta_\epsilon = 0$ , the angle  $\bar{\theta}$  is determined as

$$\bar{\theta} = \frac{\pi}{2}n, \quad (4.28)$$

with  $n$  taking an integer value. Much involved vacuum structure than Eq. (4.28) can be obtained if we take nontrivial value of  $\theta_\epsilon$ . Especially, in this case, the mass eigenstates arising from  $S$  and  $P$  fields do *not* necessary align to the VEV direction. The misalignment between the VEVs and the particle mass eigenstates causes interesting phenomenologies in this setup.

It is a bit tedious but straightforward to obtain the low energy effective theory by integrating out the  $S$  and  $P$  fields around the vacuum at the tree level. Due to the complex structure of the vacuum, Eq. (4.26), the dark quarks acquire a complex mass in general, which can be rotated away by performing an appropriate chiral rotation in the dark quark fields.

Hereafter, we take

$$\epsilon_\Delta = 0.01, \quad |\epsilon| = 0.1, \quad 0 < \theta_\epsilon < \frac{\pi}{4} \quad (4.29)$$

$$\lambda \geq 0.1. \quad (4.30)$$

Figure 13 shows the behavior of

$$R = \frac{f}{m_{\pi_D}} \frac{g_{\pi_D \pi_D \phi^\dagger \phi}}{g_{\pi_D^3 \phi^\dagger \phi}}. \quad (4.31)$$

We see it is possible to take sufficiently large value of  $g_{\pi_D \pi_D \phi^\dagger \phi} / g_{\pi_D^3 \phi^\dagger \phi}$ , if we take the parameter  $\theta_\epsilon$  small enough. Note that a  $Z_2$  symmetry ( $P \rightarrow -P$  symmetry) is restored in the  $\theta_\epsilon \rightarrow 0$  limit. The smallness of  $g_{m \phi^\dagger \phi}$  coupling ( $g_{\pi_D^3 \phi^\dagger \phi}$

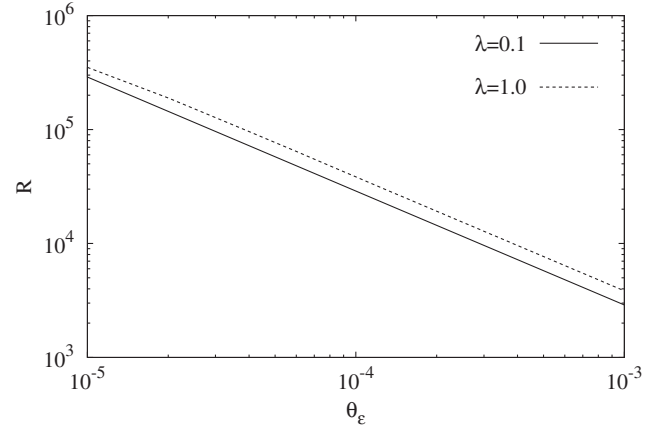


FIG. 13. The behavior of Eq. (4.31).

coupling), as we assumed in our numerical demonstrations of Sec. III, can thus be explained in a technically natural manner by the smallness of the  $\theta_\epsilon$  parameter.

## V. SUMMARY AND OUTLOOK

We have demonstrated in this article that the secluded DM scenario can successfully explain the observed relic DM density in the Universe even in the case with the non-negligibly heavy mediator particle  $m$  compared with the DM particle  $d$  mass,  $m_d \sim m_m$ , if the mediator lifetime is short enough and the  $dd \leftrightarrow mm$  transition occurs rapidly enough. The assumption  $m_d \gg m_m$  imposed in the original secluded DM scenario [18,19] is therefore not necessarily required. Allowing a heavy mediator having the mass  $m_m$  nearly degenerate with the DM particle mass  $m_d$ , novel possibilities of particle theory DM model buildings are now opened. We gave a concrete renormalizable DM model, in which both the DM particle  $d$  and the mediator particle  $m$  are realized as the dark  $SU(2)$  triplet pseudo-Nambu-Goldstone particles produced in the dark chiral symmetry breaking in the dark QCD. The rapid transition  $dd \leftrightarrow mm$  required in this scenario is naturally achieved thanks to the compositeness of the dark pions ( $d$  and  $m$ ) and the dark strong dynamics.

Although we concentrated on the computations of the relic abundance in this manuscript, much work need to be done in the DM phenomenologies in this scenario. Due to the smallness of the DM coupling with the SM sector, the direct detection of the secluded DM and the production of the DM particles in the high energy collider experiments become rather challenging. The large  $dd \rightarrow mm$  amplitude and the subsequent decay of the mediator particle  $m$ , on the other hand, induce interesting signals in the indirect astrophysical DM detection experiments. The dark pion model we proposed in this paper can easily incorporate the DM particle number decreasing mechanism through the  $3 \rightarrow 2$  scattering via the WZW interaction (SIMP mechanism) in addition to the DM number decreasing from the

mediator decay. These issues will be discussed in a separate publication.

### ACKNOWLEDGMENTS

We thank Fumihiro Takayama, Paolo Gondolo and Shigeki Matsumoto for useful discussions and valuable comments. This work is supported in part by the JSPS Grant-in-Aid for Scientific Research 15K05047 (M. T.) and 16K05325 and 16K17693 (M. Y.).

*Note added.*—During the completion stage of this manuscript, two papers [42,43] which discuss massive mediator in the cannibal DM scenario appeared in the arXiv.

### APPENDIX: TERRACE STRUCTURE STUDIED IN A SEMIANALYTIC MANNER

In this appendix, we study the terrace structure we numerically found in Sec. III A more closely using an analytic method. A semianalytic formula to evaluate the DM relic abundance  $Y_d^{\text{relic}}$  is also given. We assume the mediator  $m$  and the DM  $d$  are degenerate in mass,  $m_d = m_m$ , as in Sec. III A. They also possess the same size couplings with the SM Higgs field,  $g_{mm\phi^\dagger\phi} = g_{dd\phi^\dagger\phi}$ , thus  $\langle\sigma v\rangle_{dd\leftrightarrow\phi^\dagger\phi} = \langle\sigma v\rangle_{mm\leftrightarrow\phi^\dagger\phi}$ . The total number of relativistic degrees of freedom  $g_*$  is taken to be  $g_* = 106.75$ .

We first consider the fake freeze-out, the decoupling of the DM-mediator system from the SM particles. Since the mediator decay process is not active at the fake freeze-out time scale, we can neglect the  $\langle\Gamma\rangle_{m\leftrightarrow\phi^\dagger\phi}$  term in the Boltzmann equation (2.10). We also know  $n_d \approx n_m$ , ( $n_d^{\text{eq}} = n_m^{\text{eq}}$ ) and the Boltzmann equation describing the fake freeze-out behavior can be written as

$$\frac{dn_{d+m}}{dt} + 3Hn_{d+m} = -\frac{1}{2}\langle\sigma v\rangle_{dd\leftrightarrow\phi^\dagger\phi}[(n_{d+m})^2 - (n_{d+m}^{\text{eq}})^2], \quad (\text{A1})$$

with

$$n_{d+m} \equiv n_d + n_m, \quad n_{d+m}^{\text{eq}} = n_d^{\text{eq}} + n_m^{\text{eq}}. \quad (\text{A2})$$

The Boltzmann equation (A1) can be converted to a form

$$\frac{d}{dz}Y_{d+m} = -A_{\text{fake}}z^{-n-2}[(Y_{d+m})^2 - (Y_{d+m}^{\text{eq}})^2], \quad (\text{A3})$$

with  $z \equiv m_d/T$ .  $Y_{d+m}$  is defined as

$$Y_{d+m} = Y_d + Y_m, \quad Y_{d+m}^{\text{eq}} = Y_d^{\text{eq}} + Y_m^{\text{eq}}. \quad (\text{A4})$$

Here  $Y_d$  and  $Y_m$  are number densities normalized by entropy density  $s$ ,  $Y_d \equiv n_d/s$  and  $Y_m \equiv n_m/s$ . The thermal equilibrium  $Y_d$  and  $Y_m$  are

$$Y_d^{\text{eq}} = Y_m^{\text{eq}} = \frac{1}{2}az^{3/2}e^{-z}, \quad (\text{A5})$$

with

$$a \equiv \frac{45}{2\pi^4} \sqrt{\frac{\pi}{2}} \frac{1}{g_*}. \quad (\text{A6})$$

We therefore obtain

$$Y_{d+m}^{\text{eq}} = az^{3/2}e^{-z}. \quad (\text{A7})$$

The coefficient  $A_{\text{fake}}$  in Eq. (A3) comes from the  $dd \leftrightarrow \phi^\dagger\phi$  cross section,

$$\begin{aligned} A_{\text{fake}} &\equiv \frac{1}{2} \left[ \frac{z \langle\sigma v\rangle_{dd\leftrightarrow\phi^\dagger\phi} s}{H(T)} \right] \Big|_{T=m_d} \\ &= \sqrt{\frac{\pi}{45}} g_* m_d M_{\text{pl}} \sigma_{\text{fake}}^{(0)}. \end{aligned} \quad (\text{A8})$$

Here  $\sigma_{\text{fake}}^{(0)}$  is defined through

$$\frac{1}{2} \langle\sigma v\rangle_{dd\leftrightarrow\phi^\dagger\phi} = \sigma_{\text{fake}}^{(0)} \left( \frac{T}{m_d} \right)^n. \quad (\text{A9})$$

Note that the  $dd \leftrightarrow \phi^\dagger\phi$  process ( $mm \leftrightarrow \phi^\dagger\phi$  process) occurs through the  $s$  wave. We therefore use  $n = 0$  in our numerical estimates.

The freeze-out phenomenon in the type of Boltzmann equation (A3) has been extensively studied in the textbook [26]. We here only quote the results. The time scale at which  $Y_{d+m}$  starts to exhibit the fake freeze-out behavior ( $z_{\text{fake}}$ ) can be defined by

$$Y_{d+m}(z_{\text{fake}}) - Y_{d+m}^{\text{eq}}(z_{\text{fake}}) = c_{\text{fake}} Y_{d+m}^{\text{eq}}(z_{\text{fake}}), \quad (\text{A10})$$

with  $c_{\text{fake}}$  being an order 1 constant. It can be evaluated as

$$\begin{aligned} z_{\text{fake}} &= \ln [(2 + c_{\text{fake}})c_{\text{fake}}A_{\text{fake}}a] \\ &\quad - (n + 1/2) \ln (\ln [(2 + c_{\text{fake}})c_{\text{fake}}A_{\text{fake}}a]). \end{aligned} \quad (\text{A11})$$

The textbook suggests  $(2 + c_{\text{fake}})c_{\text{fake}} = n + 1$  gives the best fit. Using this value of  $c_{\text{fake}}$ ,  $n = 0$  and the set of parameters in the evolution example 1, we obtain

$$z_{\text{fake}} \approx 13.7, \quad (\text{A12})$$

which agrees with the fake freeze-out time scale shown in Fig. 1.

We next move to the final (true) freeze-out when the DM decouples from the mediator. Note that the mediator decay is already active at the age of the final freeze-out. The  $\langle\Gamma\rangle_{m\leftrightarrow\phi^\dagger\phi}$  term in Eq. (2.10) thus plays an important role.

On the other hand, the  $dd \leftrightarrow \phi^\dagger \phi$  and  $mm \leftrightarrow \phi^\dagger \phi$  are negligibly small. The Boltzmann equations can be approximated as

$$\frac{d}{dz} Y_d = -A_{ddmm} z^{-n'-2} [(Y_d)^2 - (Y_m)^2], \quad (\text{A13})$$

$$\frac{d}{dz} Y_m = -A_{ddmm} z^{-n'-2} [(Y_m)^2 - (Y_d)^2] - 4zBY_m. \quad (\text{A14})$$

Here we used  $\langle \Gamma \rangle_{\text{ID}} \ll \langle \Gamma \rangle_{\text{D}}$ . The coefficients  $A_{ddmm}$  and  $B$  are defined as

$$\begin{aligned} A_{ddmm} &= \left[ \frac{z \langle \sigma v \rangle_{dd \leftrightarrow mm} S}{H(T)} \right] \Big|_{T=m_d} \\ &= \sqrt{\frac{\pi}{45}} g_* m_d M_{\text{pl}} \sigma_{ddmm}^{(0)}. \end{aligned} \quad (\text{A15})$$

$$B = \frac{1}{8\pi} \sqrt{\frac{45}{\pi g_*}} \Gamma_{m \rightarrow \phi^\dagger \phi} \frac{M_{\text{pl}}}{m_d^2}. \quad (\text{A16})$$

We define  $\sigma_{ddmm}^{(0)}$  as

$$\langle \sigma v \rangle_{dd \leftrightarrow mm} = \sigma_{ddmm}^{(0)} \left( \frac{T}{m_d} \right)^{n'}. \quad (\text{A17})$$

We should note here that  $\sigma v$  in the  $dd \leftrightarrow mm$  process depends on the velocity  $v$  linearly in the case of  $d-m$  mass degeneracy. The parameter  $n'$  in the Boltzmann equations (A13) and (A14) should therefore be  $n' = 1/2$  [44].

Summing up (A13) and (A14), we obtain

$$\frac{d}{dz} Y_{d+m} = -4zBY_m. \quad (\text{A18})$$

Note also that  $Y_d$  tracks  $Y_m$  very closely until the final freeze-out  $z_f$ , and thus

$$Y_d \simeq Y_m \simeq \frac{1}{2} Y_{d+m}. \quad (\text{A19})$$

Equation (A18) can be solved as

$$Y_d \simeq Y_m \simeq a' \exp(-Bz^2), \quad (\text{A20})$$

for  $z < z_f$ . Here  $a'$  denotes the integral constant. We assume further that the behavior  $Y_m \simeq a' \exp(-Bz^2)$  is valid even at  $z \simeq z_f$  and solve the Boltzmann equation in the form of

$$\frac{d}{dz} Y_d = -A_{ddmm} z^{-n'-2} [(Y_d)^2 - (\tilde{Y}_d)^2], \quad (\text{A21})$$

with

$$\tilde{Y}_d \equiv a' \exp(-Bz^2), \quad (\text{A22})$$

instead of its original form (A13). The integral constant  $a'$  is determined by fitting Eq. (A20) with the numerical solution around  $z \simeq z_f$ . It can also be determined roughly through matching with the  $z_{\text{fake}}$  epoch physics as we will show later.

The freeze-out phenomenon in Eq. (A21) can now be analyzed in a manner similar to the textbook calculation of the standard cold thermal relic abundance. There are a couple of important differences in (A21), however, the fractional  $n' = 1/2$  and the  $\exp(-Bz^2)$  damping behavior of  $\tilde{Y}_d$ . We see in below how these differences affect the freeze-out phenomenon in (A21).

We introduce

$$\Delta \equiv Y_d - \tilde{Y}_d, \quad (\text{A23})$$

and define the freeze-out time scale  $z_f$  by

$$\Delta(z_f) = c_f \tilde{Y}_d(z_f), \quad (\text{A24})$$

with  $c_f$  being an order 1 constant. The Boltzmann equation (A21) can be expressed as

$$\frac{d}{dz} \Delta = -\frac{d}{dz} \tilde{Y}_d - A_{ddmm} z^{-n'-2} \Delta (2\tilde{Y}_d + \Delta), \quad (\text{A25})$$

which can be solved approximately at  $z = z_f$  as

$$\begin{aligned} \Delta(z_f) &\simeq -\frac{z_f^{n'+2}}{A_{ddmm} (2 + c_f) \tilde{Y}_d} \left. \frac{d}{dz} \tilde{Y}_d \right|_{z=z_f} \\ &= \frac{2B}{A_{ddmm}} \frac{z_f^{n'+3}}{2 + c_f}. \end{aligned} \quad (\text{A26})$$

Comparing Eq. (A26) with Eq. (A24), we obtain

$$\frac{2B}{A_{ddmm}} \frac{z_f^{n'+3}}{2 + c_f} = c_f a' \exp(-Bz_f^2), \quad (\text{A27})$$

which leads to a formula to determine the freeze-out time scale

$$\begin{aligned} z_f^2 &\simeq \frac{1}{B} \ln \left[ \frac{(2 + c_f) c_f A_{ddmm} a'}{2B} \right] \\ &\quad - \frac{n' + 3}{2} \frac{1}{B} \ln \left( \frac{1}{B} \ln \left[ \frac{(2 + c_f) c_f A_{ddmm} a'}{2B} \right] \right) \\ &\quad + \dots \end{aligned} \quad (\text{A28})$$

Note  $z_f^2$  is proportional to  $\ln A_{ddmm}$  in Eq. (A28). This is in contrast to the usual cold thermal relic computation in which  $z_f$  is proportional to  $\ln A$ . This property comes from the  $\exp(-Bz^2)$  damping behavior of  $\tilde{Y}_d$  in this scenario. We also note very slow convergence of the series expansion equation (A28). In our numerical analysis, we therefore use Eq. (A27) directly, rather than Eq. (A28).

Once we determine  $z_f$ , we can compute the relic abundance at  $z \rightarrow \infty$  by

$$Y_d^{\text{relic}} = \lim_{z \rightarrow \infty} \Delta(z). \quad (\text{A29})$$

For  $z \gg z_f$ , (A25) can be approximated as

$$\frac{d}{dz} \Delta = -A_{ddmm} z^{-n'-2} \Delta^2. \quad (\text{A30})$$

Integrating (A30) from  $z_f$  to  $\infty$ , we obtain

$$Y_d^{\text{relic}} \simeq \frac{n'+1}{A_{ddmm}} z_f^{n'+1}. \quad (\text{A31})$$

Here the initial value uncertainty  $\Delta(z_f)$  is absorbed in the uncertainty in  $z_f$ . Note (A31) is identical to the textbook formula for the cold thermal relic abundance, except for the fractional value of  $n' = 1/2$ . We obtain  $a' \simeq 8.5 \times 10^{-9}$  and  $Y_d^{\text{relic}} \simeq 4.2 \times 10^{-13}$  in our numerical analysis

presented in Sec. III A. Using these values, we see Eq. (A31) as combined with (A28) gives the best fit with

$$c_f \simeq 1.1, \quad (\text{A32})$$

which is perfectly consistent with the assumption we made on  $c_f$ : it is an order 1 constant. The corresponding freeze-out  $z_f$  is calculated as

$$z_f \simeq 564. \quad (\text{A33})$$

Again Eq. (A33) is consistent with Fig. 1.

The final task we need to carry out is to make a relation between the fake freeze-out  $z_{\text{fake}}$  and the final freeze-out  $z_f$ . This can be done by computing the coefficient  $a'$  in (A20) in terms of  $z_{\text{fake}}$ . Assuming the textbook formula

$$Y_{d+m} = \frac{(n+1)z_{\text{fake}}^{n+1}}{A_{\text{fake}}} \quad (\text{A34})$$

gives the abundance at  $z = z_{\text{fake}}$  in Eq. (A20), we see

$$a' = \frac{(n+1)z_{\text{fake}}^{n+1}}{2A_{\text{fake}}} \exp(Bz_{\text{fake}}^2). \quad (\text{A35})$$

Equation (A35) gives a result consistent with our numerical fit on  $a'$  within 40% uncertainty.

- 
- [1] K. A. Olive *et al.* (Particle Data Group Collaboration), Review of particle physics, *Chin. Phys. C* **38**, 090001 (2014).
- [2] G. Hinshaw *et al.* (WMAP Collaboration), Nine-year Wilkinson microwave anisotropy probe (WMAP) observations: cosmological parameter results, *Astrophys. J. Suppl. Ser.* **208**, 19 (2013).
- [3] P. A. R. Ade *et al.* (Planck Collaboration), Planck 2015 results. XIII. Cosmological parameters, *Astron. Astrophys.* **594**, A13 (2016).
- [4] G. Bertone, D. Hooper, and J. Silk, Particle dark matter: Evidence, candidates and constraints, *Phys. Rep.* **405**, 279 (2005).
- [5] J. L. Feng, Dark matter candidates from particle physics and methods of detection, *Annu. Rev. Astron. Astrophys.* **48**, 495 (2010).
- [6] B. W. Lee and S. Weinberg, Cosmological Lower Bound on Heavy Neutrino Masses, *Phys. Rev. Lett.* **39**, 165 (1977).
- [7] T. Marrodán Undagoitia and L. Rauch, Dark matter direct-detection experiments, *J. Phys. G* **43**, 013001 (2016).
- [8] D. Abercrombie *et al.*, Dark matter benchmark models for early LHC Run-2 searches: Report of the ATLAS/CMS dark matter forum, [arXiv:1507.00966](https://arxiv.org/abs/1507.00966).
- [9] A. Tan *et al.* (PandaX-II Collaboration), Dark Matter Results from First 98.7 Days of Data from the PandaX-II Experiment, *Phys. Rev. Lett.* **117**, 121303 (2016).
- [10] A. Manalaysay, Dark-matter results from 332 new live days of LUX data, in IDM2016, The University of Sheffield, Sheffield, UK, 2016 (unpublished).
- [11] D. S. Akerib *et al.*, Results from a search for dark matter in the complete LUX exposure, *Phys. Rev. Lett.* **118**, 021303 (2017).
- [12] P. Agnes *et al.* (DarkSide Collaboration), Results from the first use of low radioactivity argon in a dark matter search, *Phys. Rev. D* **93**, 081101 (2016).
- [13] R. Agnese *et al.* (SuperCDMS Collaboration), Improved WIMP-search reach of the CDMS II germanium data, *Phys. Rev. D* **92**, 072003 (2015).
- [14] Y. Hochberg, E. Kuflik, T. Volansky, and J. G. Wacker, Mechanism for Thermal Relic Dark Matter of Strongly Interacting Massive Particles, *Phys. Rev. Lett.* **113**, 171301 (2014).
- [15] Y. Hochberg, E. Kuflik, H. Murayama, T. Volansky, and J. G. Wacker, Model for Thermal Relic Dark Matter of Strongly Interacting Massive Particles, *Phys. Rev. Lett.* **115**, 021301 (2015).

- [16] J. Wess and B. Zumino, Consequences of anomalous Ward identities, *Phys. Lett.* **B37**, 95 (1971).
- [17] E. Witten, Global aspects of current algebra, *Nucl. Phys.* **B223**, 422 (1983).
- [18] M. Pospelov, A. Ritz, and M. B. Voloshin, Secluded WIMP dark matter, *Phys. Lett. B* **662**, 53 (2008).
- [19] N. Arkani-Hamed, D. P. Finkbeiner, T. R. Slatyer, and N. Weiner, A theory of dark matter, *Phys. Rev. D* **79**, 015014 (2009).
- [20] D. Pappadopulo, J. T. Ruderman, and G. Trevisan, Dark matter freeze-out in a nonrelativistic sector, *Phys. Rev. D* **94**, 035005 (2016).
- [21] A. Berlin, D. Hooper, and G. Krnjaic, PeV-scale dark matter as a thermal relic of a decoupled sector, *Phys. Lett. B* **760**, 106 (2016).
- [22] V. Silveira and A. Zee, Scalar phantoms, *Phys. Lett.* **161B**, 136 (1985).
- [23] J. McDonald, Gauge singlet scalars as cold dark matter, *Phys. Rev. D* **50**, 3637 (1994).
- [24] C. P. Burgess, M. Pospelov, and T. ter Veldhuis, The minimal model of nonbaryonic dark matter: A singlet scalar, *Nucl. Phys.* **B619**, 709 (2001).
- [25] G. Belanger and J. C. Park, Assisted freeze-out, *J. Cosmol. Astropart. Phys.* **03** (2012) 038.
- [26] E. W. Kolb and M. S. Turner, The early universe, *Front. Phys.* **69**, 1 (1990).
- [27] P. Bandyopadhyay, E. J. Chun, and J. C. Park, Right-handed sneutrino dark matter in  $U(1)'$  seesaw models and its signatures at the LHC, *J. High Energy Phys.* **06** (2011) 129.
- [28] Y. Bai and R. J. Hill, Weakly interacting stable hidden sector pions, *Phys. Rev. D* **82**, 111701 (2010).
- [29] M. R. Buckley and E. T. Neil, Thermal dark matter from a confining sector, *Phys. Rev. D* **87**, 043510 (2013).
- [30] S. Bhattacharya, B. Melić, and J. Wudka, Pion dark matter, *J. High Energy Phys.* **02** (2014) 115.
- [31] T. A. Ryttov and F. Sannino, Ultraminimal technicolor and its dark matter technicolor interacting massive particles, *Phys. Rev. D* **78**, 115010 (2008).
- [32] M. Frigerio, A. Pomarol, F. Riva, and A. Urbano, Composite scalar dark matter, *J. High Energy Phys.* **07** (2012) 015.
- [33] A. Carmona and M. Chala, Composite dark sectors, *J. High Energy Phys.* **06** (2015) 105.
- [34] T. Hur and P. Ko, Scale Invariant Extension of the Standard Model with a Strongly Interacting Hidden Sector, *Phys. Rev. Lett.* **106**, 141802 (2011).
- [35] Y. Ametani, M. Aoki, H. Goto, and J. Kubo, Nambu-Goldstone dark matter in a scale invariant bright hidden sector, *Phys. Rev. D* **91**, 115007 (2015).
- [36] H. Hatanaka, D. W. Jung, and P. Ko, AdS/QCD approach to the scale-invariant extension of the standard model with a strongly interacting hidden sector, *J. High Energy Phys.* **08** (2016) 094.
- [37] M. Holthausen, J. Kubo, K. S. Lim, and M. Lindner, Electroweak and conformal symmetry breaking by a strongly coupled hidden sector, *J. High Energy Phys.* **12** (2013) 076.
- [38] Y. Hochberg, E. Kuflik, and H. Murayama, SIMP spectroscopy, *J. High Energy Phys.* **05** (2016) 090.
- [39] R. S. Chivukula and T. P. Walker, Technicolor cosmology, *Nucl. Phys.* **B329**, 445 (1990).
- [40] M. Farina, Asymmetric twin dark matter, *J. Cosmol. Astropart. Phys.* **11** (2015) 017.
- [41] M. Freytsis, S. Knapen, D. J. Robinson, and Y. Tsai, Gamma-rays from dark showers with twin Higgs models, *J. High Energy Phys.* **05** (2016) 018.
- [42] M. Farina, D. Pappadopulo, J. T. Ruderman, and G. Trevisan, Phases of cannibal dark matter, *J. High Energy Phys.* **12** (2016) 039.
- [43] J. A. Dror, E. Kuflik, and W. H. Ng, Codecaying Dark Matter, *Phys. Rev. Lett.* **117**, 211801 (2016).
- [44] K. Griest and D. Seckel, Three exceptions in the calculation of relic abundances, *Phys. Rev. D* **43**, 3191 (1991).